



Performance of the WRF model in simulating convective rainfall events in the humid subtropical monsoon climate region—Poyang Lake basin

Jinru Wu¹ · Jianzhong Lu¹ · Xiaoling Chen¹

Received: 19 December 2022 / Accepted: 25 May 2023 / Published online: 7 June 2023

© The Author(s), under exclusive licence to Springer-Verlag GmbH Austria, part of Springer Nature 2023

Abstract

The Weather Research and Forecasting (WRF) model can provide high-resolution rainfall and is important for flood management and prevention. In order to evaluate the performance of WRF and select the best combination of physical parameterizations, as well as exploring how cumulus parameterizations influence the rainfall simulation at 3-km grid spacing over the Poyang Lake basin, the WRF model was configured with horizontal grid spacing of 27, 9, and 3 km using the three microphysical parameterizations (MPs), three cumulus parameterizations (CUs), and two planetary boundary layer parameterizations (PBLs) for three representative 24-h rainfall events. Results show that (1) the selection of physical parameterizations has a greater influence than horizontal grid spacing on rainfall simulation. The maximum relative error (RE) difference between three domains is 2.51%, 1.11%, and 2.52% for three rainfall events, while that for R1 to R3 is 29.13%, 26.68%, and 39.89%, respectively. (2) Among 18 schemes, S11, containing parameterizations of New Thompson and YSU, shows overall better performance for spatial and temporal rainfall simulation. S5, containing parameterizations of WSM6 and YSU, and S15, containing parameterizations of Morrison and YSU, are also good choices for rainfall simulation. (3) In most cases, the use of cumulus schemes at 3-km resolution does not show obvious advantages over these not use cumulus schemes in rainfall forecasts. (4) The numerical simulations are more sensitive to the selection of PBLs than MPs in the study area. Among individual parameterizations, YSU is the best choice for PBLs in simulating rainfall. Overall, the results demonstrated that WRF can provide useful rainfall simulation, and the study provides a reference in rainfall forecast using WRF over the Poyang Lake basin.

1 Introduction

Influenced by global climate change, the frequency and intensity of extreme rainfall show an increased trend (Spinoni et al. 2020; H. Afshar et al. 2020; Schiermeier 2011), which often triggers floods that have damaging societal impacts (Muis et al. 2016; Mohanty et al. 2020; Zhai et al. 2005). Rainfall estimation and forecast in a particular area are essential to flood management and prevention. However, rainfall is characterized by a highly heterogeneous process both in time and space in regions with complex topography (Nicótina et al. 2008), making it challenging to

forecast spatial and temporal variations of rainfall with high accuracy (Piciullo et al. 2018; Amjad et al. 2020; Liu et al. 2020a).

In recent years, numerical weather prediction (NWP) models have been wildly applied in rainfall forecast (Litta et al. 2012; Pennelly et al. 2014; Patel et al. 2019; Zhuo et al. 2019), and they have been proven to provide reliable rainfall estimation at spatial and temporal resolutions (Rasmussen et al. 2011; Prein et al. 2013). Among various NWP models, the Weather Research and Forecasting (WRF) model has shown more reasonable skill in reproducing precipitation distribution and intensity patterns over complex terrain (Argüeso et al. 2011; Maussion et al. 2011; Cossu et al. 2014; Li et al. 2016; Hasan et al. 2018; Liu et al. 2020b). Previous studies have demonstrated that the selection of different physical parameterizations can directly influence the success of WRF predictability and have attracted most attention (Shrestha et al. 2013; Sunny Lim et al. 2014; Di et al. 2015; Dyer et al. 2016; Song et al. 2017; Singh et al. 2018; Houze 2006; Bossoli et al. 2009), among which

✉ Jianzhong Lu
lujzhong@whu.edu.cn

¹ State Key Laboratory of Information Engineering in Surveying, Mapping and Remote Sensing, Wuhan University, Wuhan 430079, China

parameterizations of microphysics (MP), cumulus (CU), and planetary boundary layer (PBL) are mostly discussed (Hong et al. 2009; Madala et al. 2014; Cassola et al. 2015; Dasari et al. 2015; Kan et al. 2015; Pieri et al. 2015). According to Duzenli et al. (2020), the precipitation estimates over the Eastern Black Sea and Mediterranean regions in Turkey are mostly driven by MP schemes, especially for autumn precipitation. They also found that PBL and CU schemes highly depend on rainfall timing and location. However, another study by Argüeso et al. (2011) done over regions with complex terrain and a Mediterranean climate shows that CU and PBL have a noticeable influence in describing precipitation extremes, while MP schemes have a minor impact on the description of precipitation. Similarly, a study carried out over West Africa by Flaounas et al. (2011) pointed out that PBL is most influential on rainfall amount and CU has the greatest impact on rainfall variability. Yang et al. (2020) reproduced five intense precipitation events in summer over the Hanjiang River Basin (HRB) in China using WRF and found that the precipitation simulation is substantially driven by CU schemes and it is less sensitive to the choice of the MP schemes. Que et al. (2016) compared different CU, PBL, and MP schemes in the WRF model over the Asian summer monsoon region, and results showed that the choice of PBL scheme has a significant effect on precipitation in such a large area. Taraphdar and Pauluis (2021); Taraphdar et al. (2021) explored the impact of PBL and MP schemes on the sensitivity of monsoon rainfall over the Indian region, and they found that PBL schemes dramatically impact the rainfall simulation. These studies indicated that the performance of different physical schemes on rainfall simulation varied with different regions and climates. In the WRF model, there are many MP options, PBL options, CU options, and other physical options, which can make up hundreds of combinations of physical parameterizations. Therefore, before applying the WRF model for predication, a sensitivity study and evaluation of numerous combinations should be conducted over specified regions to access the optimal option (Mannan et al.).

The WRF domain configuration is another influential factor in rainfall simulation, such as the horizontal resolution (Li et al. 2008; Dyer et al. 2016). Generally speaking, WRF runs with fine grid spacing can achieve good performance due to their ability to resolve more small-scale features. But many studies show that at a resolution within 10 km, the WRF simulations with reducing horizontal grid spacing do not perform better than those with increasing horizontal grid spacing (Schwartz et al. 2009; Tian et al. 2017; Duzenli et al. 2020). In addition, some studies suggested that the cumulus parameterization at high horizontal resolutions should be turned off, where deep convection is partly resolved, thus enabling the removal of convective parameterization (Yu and Lee 2010). However, there are still numerous recent studies that have used the cumulus parameterization

schemes in the WRF simulations at a grid spacing less than 4 km (Tian et al. 2017; Chawla et al. 2018; Yang et al. 2020; Tian et al. 2021). Whether the convective schemes are needed at high horizontal spatial resolutions has not reached a consistent conclusion. As the meaning of downscaling and the high-resolution model is usually necessary in meteorological and hydrological studies, it is essential to examine how cumulus parameterization schemes influence the high-resolution numerical rainfall simulation.

With this perspective, three destructive rainfall events are reproduced by WRF-ARW in the humid subtropical monsoon climate zone—the Poyang Lake basin. The aims of the study include the following: (1) investigate the influence of WRF horizontal grid spacing on the rainfall simulation and evaluate how the cumulus parameterization influences the rainfall simulation on the 3-km grid spacing. (2) Select the optimal physical parameterization schemes for rainfall simulations over the monsoon region and explore the sensitivity of WRF physical parameterizations.

2 Study area and WRF model setup

2.1 Study area

Poyang Lake basin ($24^{\circ} 28' \text{--} 30^{\circ} 05'$ N, $113^{\circ} 33' \text{--} 118^{\circ} 29'$ E) is located in a humid subtropical monsoon climate zone, covering $162,200 \text{ km}^2$ in area (Liang et al. 2020), which covers about 97% of the Jiangxi provincial territory (Tang et al. 2018). Characterized by complex topography, the study area is surrounded by mountains on three sides from east to west, with undulating hills in the middle, and the Poyang Lake Plain in the north (Fig. 1). The mountains account for 36% of the total area, the hills account for 42%, and the plains and water area account for 22%. The Poyang Lake basin consists of five main river sub-basins, including the Gan basin, Fu basin, Xin basin, Rao basin, Xiu basin, and the Poyang Lake plain. This area is affected by both south-east and south-west monsoons; the average annual temperature in the basin is 17.5°C ; the average annual cumulative precipitation (daily precipitation $\geq 0.1 \text{ mm/day}$) frequency is 192 days; and the annual average precipitation is 1638 mm (Liu et al. 2020a). Besides, the rainfall occurs mainly from April to September, accounting for about 75% of the annual rainfall in total.

2.2 WRF model configuration

The WRF-ARW is a compressible, non-hydrostatic, meteorological model and data assimilation system (Skamarock et al. 2008). In this study, the WRF-ARW version 4.0 is used to conduct the rainfall simulation, and three model domains with two-way nesting are configured with the downscaling

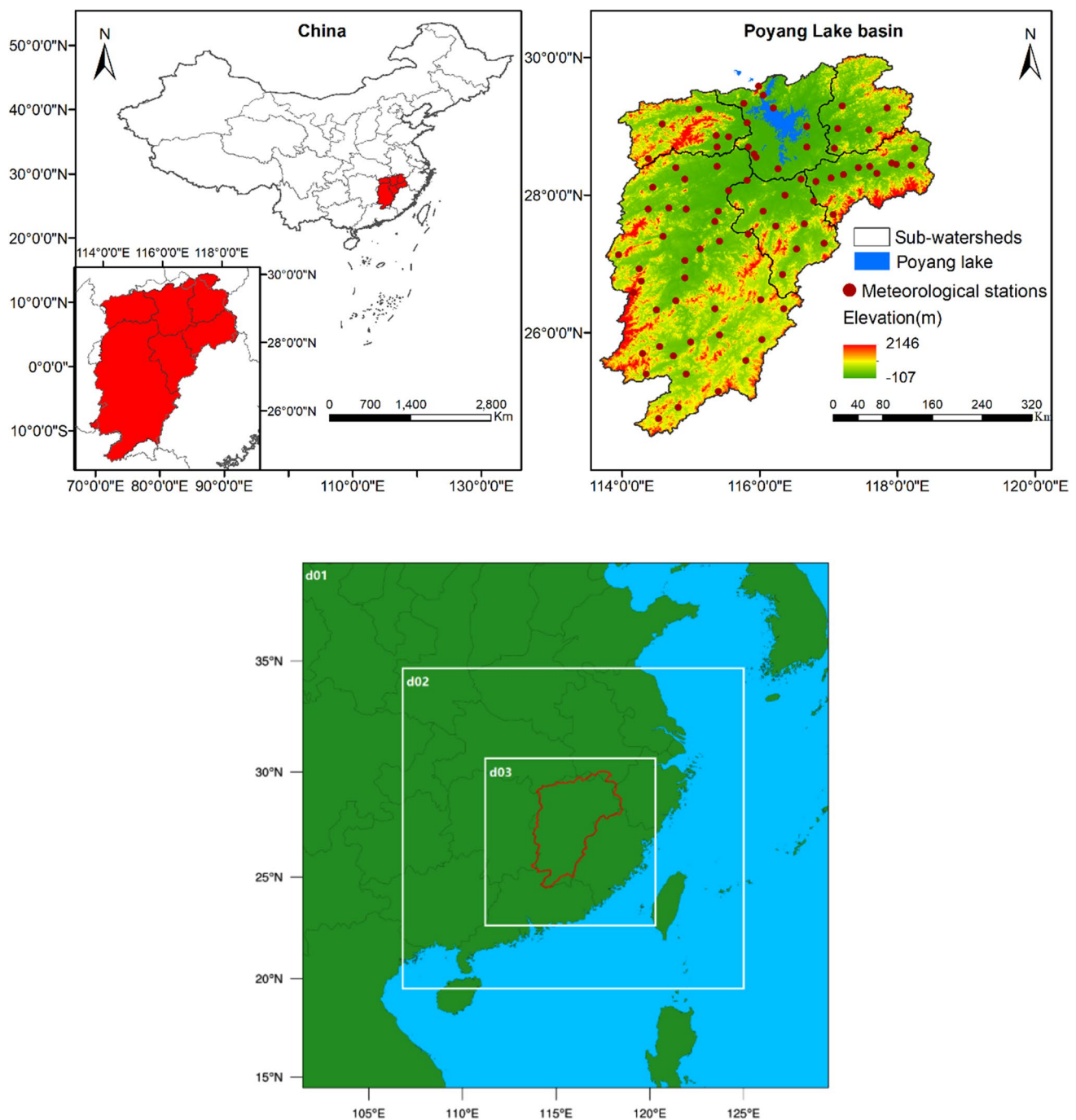


Fig. 1 The location map of the Poyang Lake basin with different domain sizes

ratio of 1:3:3. The horizontal resolution of the outmost domain (D01) is 27 km with grid numbers of 101×101 . The child of D01, the middle domain D02, is set to 9 km with grid numbers of 196×184 . The innermost domain, covering the Poyang Lake basin completely, has a horizontal resolution of 3 km with grid numbers of 292×292 . In

general, initial conditions have a large impact on precipitation forecasts, and global final analysis data (FNL) is one of the commonly used driving data for simulating historical rainfall events (Kim et al. 2013), as FNL is closer to actual atmospheric conditions. So FNL with a horizontal resolution of 1×1 at 6 h intervals—00:00, 06:00, 12:00, and 18:00

Table 1 WRF configurations for rainfall simulations

Physical parameterization schemes	MP	CU	PBL
S1	WSM6	KF	YSU
S2	WSM6	KF	MYJ
S3	WSM6	BMJ	YSU
S4	WSM6	BMJ	MYJ
S5	WSM6	Grell-3	YSU
S6	WSM6	Grell-3	MYJ
S7	New Thompson	KF	YSU
S8	New Thompson	KF	MYJ
S9	New Thompson	BMJ	YSU
S10	New Thompson	BMJ	MYJ
S11	New Thompson	Grell-3	YSU
S12	New Thompson	Grell-3	MYJ
S13	Morrison	KF	YSU
S14	Morrison	KF	MYJ
S15	Morrison	BMJ	YSU
S16	Morrison	BMJ	MYJ
S17	Morrison	Grell-3	YSU
S18	Morrison	Grell-3	MYJ

UTC—is used as the initial and lateral boundary conditions for the WRF rainfall simulations. The model spin-up time in this study is set to 6 h, and the model results are output hour by hour, as studies have shown that a spin-up time of 6 h can develop smaller-scale convective features (Kain et al. 2010). For each rainfall event, a 30-h simulation is performed, and the first spin-up time of 6 h is discarded from the analysis.

A number of combinations of physical parameterizations have been used to access rainfall products worldwide. MP schemes mainly control the water vapor, cloud, and precipitation process (Sikder et al. 2016). Chawla et al. (2018) found that in the western Himalayas, the Goddard scheme outperformed other microphysics schemes in rainfall simulation. Kim et al. (2013) have tested the sensitivity of six microphysics schemes to two typhoon rainstorm events in Korea, and the rainfall simulated from the WRF Single-Moment 6 (WSM6) scheme (Hong and Lim 2006) and the WRF Double-Moment 6 (WDM6) scheme (Lim and Hong, 2010) fitted well with observed data, while Lin et al. (1983) and New Thompson et al. (2004) should be avoided to choose in the convective rainfall areas. Among a series of WSM schemes that were widely used in China, WSM6 including the mixing ratios of water vapor, cloud water, cloud ice, snow, rain, and graupel is more efficient than WSM5 (Hong et al. 2006). The New Thompson scheme is a well-known double-moment bulk scheme with ice, snow, and graupel processes suitable for high-resolution simulations (Cassola et al. 2015). The Morrison scheme (Morrison et al. 2009) has double-moment ice, snow, rain, and graupel

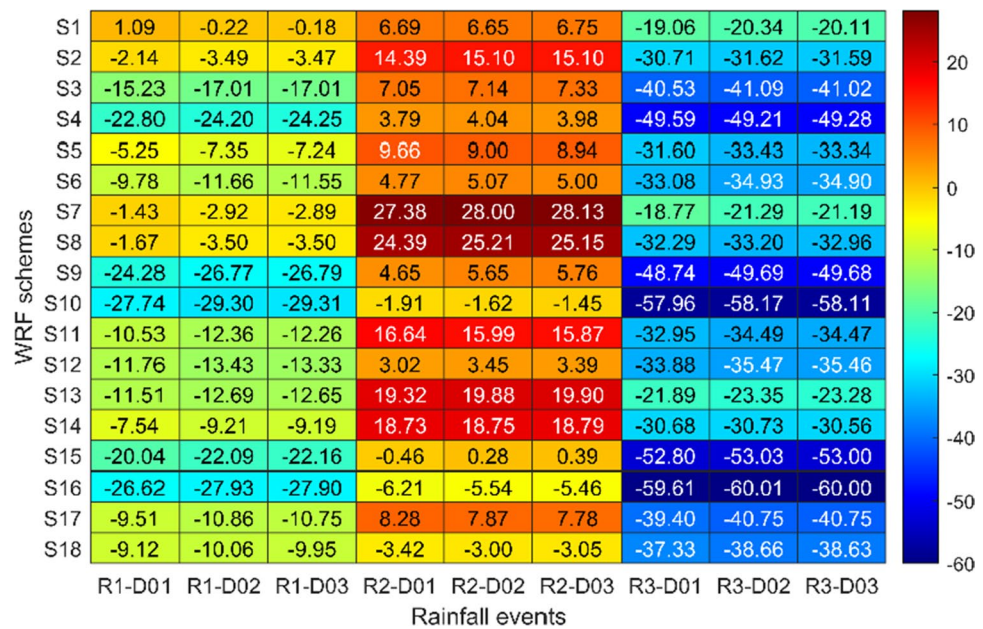
for cloud-resolving simulations, which is suitable for finer resolutions while simulated inside the WRF model. Liu et al. (2020b) evaluated the capacity of four microphysics schemes for rainfall simulation in the Tianshan Mountains, and they found that WSM6 is the most appropriate choice. CU schemes are responsible for redistributing atmospheric heat and moisture (Huang et al. 2017), and the rainfall process is greatly influenced by the cumulus convection process with cloud generation and evolution (Tian et al. 2021). Kain-Fritsch (KF) scheme (Kain and Fritsch 1993), and Betts-Miller-Janjic (BMJ) scheme (Janjic 1994), and Grell-Devenyi (GD) scheme (Grell and Devenyi 2002) are widely used CU schemes. The KF scheme is a mass-flux parameterization scheme which triggers deep convection when a mixed parcel has positive vertical velocity over a depth such as 3 to 4 km (Kain, 2004). The BMJ scheme deduces the convective processes from the reference temperature and moisture profiles (Janjic 1994). Both the KF and BMJ schemes can simulate deep and shallow convection phenomena. The Grell 3 scheme makes use of ensemble parameterization with different closure assumptions and parameters, and it is more suitable for grid sizes less than 10 km, as it spreads subsidence effects to neighboring grid columns (Grell and Devenyi 2002). KF and BMJ were chosen by Argüeso et al. (2011) to evaluate the performance for rainfall simulation over Spain. The results showed that BMJ performed best. The performance of KF and GD for rainfall simulation in North America was also tested by Pei et al. (2014), and they found the error between simulated rainfall and observed rainfall in the GD scheme is smaller.

PBL schemes have a direct impact on vertical mixing and are responsible for modulating the mixed layer depth as well as associated moisture availability (Verma et al. 2021; Sathyamadhan et al. 2017; Misenis and Yang 2010). Yonsei University (YSU) scheme (Hong et al. 2006) and Mellor-Yamada-Janjic (MYJ) scheme (Janjic 2001) are the two most widely used planetary boundary solutions (Tian et al. 2017). The YSU is a first-order non-local scheme with

Table 2 The characteristics of three selected rainfall events

Rainfall no.	Storm start time	Storm end time	24-h accumulated areal rainfall (mm)
R1	19/06/2010 08:00	20/06/2010 08:00	71.17
R2	14/06/2011 14:00	15/06/2011 14:00	51.92
R3	06/06/2019 08:00	07/06/2019 08:00	47.96

Fig. 2 The RE values (%) in three domains for three rainfall events



a counter-gradient term in the eddy-diffusion equation to represent fluxes due to non-local gradients. While MYJ is a local closure scheme, it uses the 1.5 order turbulence closure model of Mellor and Yamada to represent turbulence above the surface layer. The simulated rainfall of the scheme including the MYJ parameter is found to be less than that of the YSU over East Africa (Flaounas et al. 2011).

To have a useful benchmark with previous works, the physical parameterizations we selected were widely discussed in similar studies. Therefore, three microphysics schemes (WSM6,

New Thompson, Morrison), three cumulus convection schemes (KF, BMJ, Grell-3), and two planetary boundary layer schemes (YSU, MYJ) were selected and combined into 18 physical parameterization schemes as shown in Table 1, which were considered for three rainfall event simulation. In addition, the RRTM long-wave radiation scheme (Mlawer et al. 1997), the Dudhia short-wave radiation scheme (Dudhia 1989), and the Noah land-surface scheme (Chen and Dudhia 2001) were used. Although high horizontal resolution can resolve convective processes explicitly, there is no univocal conclusion about the

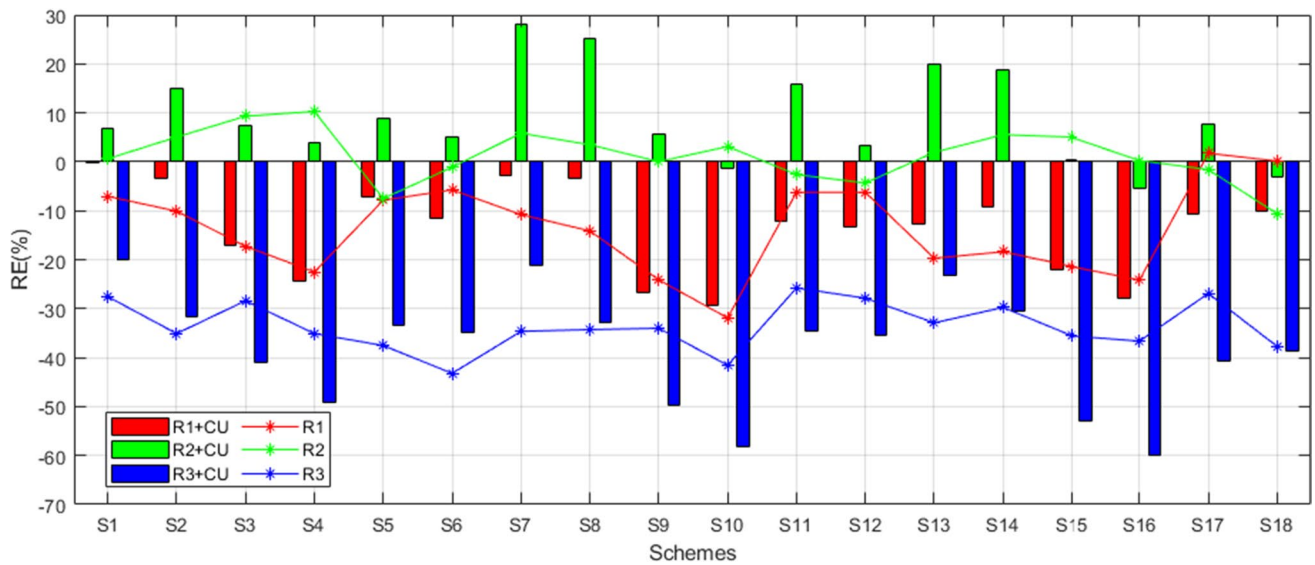


Fig. 3 Comparison of rainfall simulations for three rainfall events with CU and without CU based on RE

threshold of the high horizontal resolution that whether convective parameterization is needed. What is more, convective parameterization is proved to be helpful at even less than 3-km horizontal resolution in producing realistic rainfall structures (Li and Pu 2009). Therefore, to make our study more convincing, experiments both with and without cumulus parameterization on the 3-km grid spacing were conducted to examine the impact of cumulus parameterizations of the WRF model on rainfall simulations in 3 km over the Poyang Lake basin.

2.3 Rainfall events

Three rainfall events with different characteristics numbering from R1 to R3 were considered in the Poyang Lake basin, and all of them are convective rainfall, and the synoptic description of these rainfall events can be referred to previous works (Zhou et al. 2012; Sun et al. 2015; Ling et al. 2020). R1 was formed on June 19, 2010. Affected by the weak cold air in the north, the warm and humid airflow at the edge of the subtropical high, and the eastward shift of the southwest vortex, heavy rain generally occurred in the north-central part of Jiangxi Province (Zhou et al. 2012). Occurred on June 14, 2011, R2 was caused by the combined influence of the forward-dipping trough, the warm and humid airflow from the southwestern edge of the subtropical high pressure, and the cold air (Sun et al. 2015). R3 was formed on June 6, 2019. It was a continuous torrential rain, which was mainly caused by the high-altitude northwest airflow (Ling et al. 2020). The daily rainfall generally reached the torrential

rain standard or the heavy torrential rain standard, and there was extremely heavy torrential rain locally.

The basic information of three selected rainfall events is shown in Table 2.

3 Data and methodology

3.1 Observed data

In order to evaluate the performance of the WRF model, the hourly rainfall data over the Poyang Lake basin from 80 meteorological stations were used, which can be downloaded from the China Meteorological Data Service Center. For comparison, the WRF grid points were interpolated to the observation points using the inverse distance weight interpolation method.

3.2 Verification strategy

3.2.1 Relative error (RE)

Areal rainfall refers to the amount of rainfall in a certain area in a specific time period, which can objectively reflect the rainfall in the entire region. Heavy rainfall with an areal rainfall greater than the critical value is the direct factor leading to floods. The relative error (RE) was used to evaluate the accuracy of simulated areal rainfall, and RE is calculated by Eq. (1):

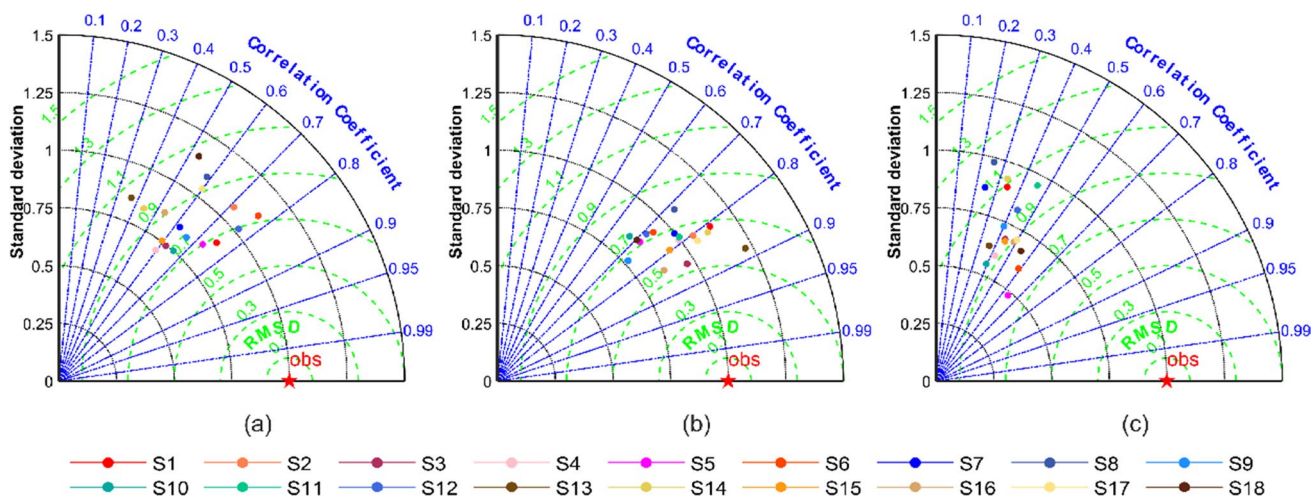


Fig. 4 Taylor diagrams of 18 spatial simulations and observations for R1 (a), R2 (b), and R3 (c)

Sensitivity of the Weather Research and Forecasting (WRF) model to downscaling ratios and storm types in rainfall simulation

Sensitivity of the Weather Research and Forecasting (WRF) model to downscaling ratios and storm types in rainfall simulation

$$RE = \frac{S - O}{O} \times 100\% \quad (1)$$

where S and O represent simulated and observed 24-h accumulated areal rainfall, respectively. The former is calculated by averaging 24-h accumulated rainfall from all grids inside the Poyang Lake basin, and the latter is calculated using the Thiessen polygon method (Jarvis et al. 2013) with the observed accumulated rainfall of 80 meteorological stations in the Poyang Lake basin. The perfect score is 0 for RE.

3.2.2 Taylor diagram

The Taylor diagram (Taylor 2001) method is used to evaluate the ability in reproducing the spatial and temporal pattern of the rainfall, which can summarize the model performance between the model simulations and the observation using three pairwise comparison statistics, including the correlation coefficient (R), the ratio of standard deviation (SD), and the centered pattern root-mean-square difference (C-RMSD) (Taylor 2001; Sanchez et al. 2012). The R and C-RMSD are the quantities that measure the degree of phase agreement of two fields and the degree of agreement in amplitude, respectively. The perfect scores of R and SD are 1, while that of C-RMSD is 0.

3.2.3 CRI

Different statistics evaluate the performance of WRF schemes on different aspects; therefore, considering both spatial and temporal skills of the schemes in rainfall simulation, the comprehensive rating index (CRI) is used to effectively rank schemes (Jiang et al. 2015) and determine the optimal physical parameterization. The equation is as follows:

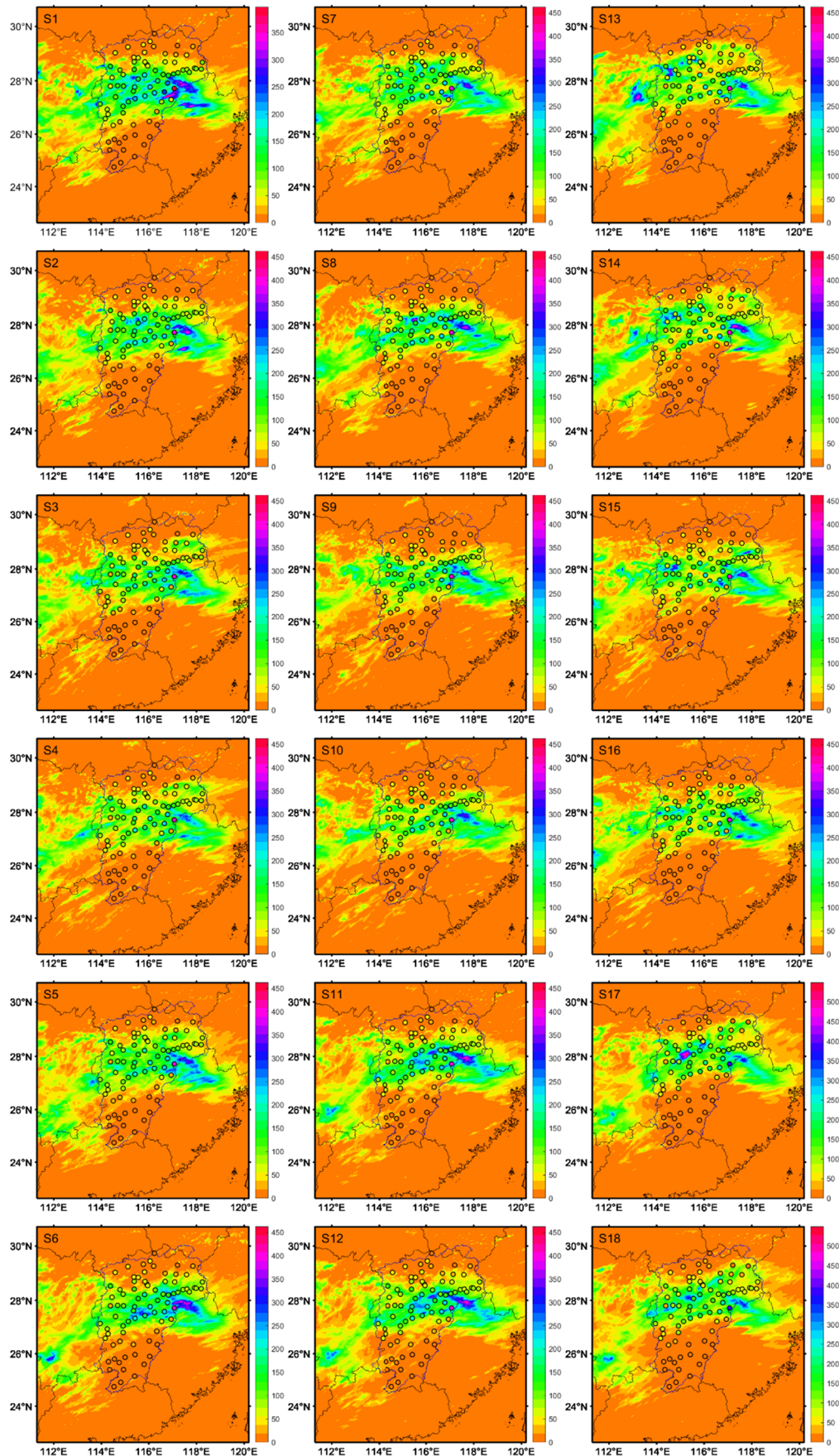
$$CRI = 1 - \frac{1}{m \times n} \sum_{i=0}^n \text{rank}_i \quad (2)$$

where m represents the number of schemes (18) and n is the number of statics used (6). The perfect score of CRI is 1.

4 Results and discussion

4.1 Influence of horizontal resolution on the accumulated areal rainfall simulations

The accumulated areal rainfall for the three rainfall events was simulated by 18 WRF schemes in three domains, and the 18 simulations were evaluated using RE. Those areal rainfall results of 27 km, 9 km, and 3 km horizontal resolutions were obtained from the same simulations as the 27-9-3 km domain simulations. In Fig. 2, the Y-axis refers to 18 schemes numbered from S1 to S18, and the X-axis refers to different domains of three rainfall events. For example, R1-D01 represents results from domain 1 of R1. According to RE values, the total rainfalls for R1 and R3 are generally underestimated in WRF schemes, while those for R2 are generally overestimated. This indicates that rainfall types may have an impact on WRF rainfall simulations. And further work should be conducted to identify if the bias has clear patterns with different rainfall types and how to correct it. The best and worst schemes at different resolutions are consistent for a single rainfall event. Regarding the RE values of a certain rainfall event, there is a slight difference between the three domains, and the maximum difference between the three domains is 2.51%, 1.11%, and 2.52% for R1 to R3, respectively. In addition, results show that increasing the horizontal resolution does not always lead to an improvement of areal rainfall simulation. When the horizontal resolution is increased from 27 to 9 km, the absolute RE increases. In contrast, when the horizontal resolution is increased from 9 to 3 km, the absolute RE decreases. However, a significant difference can be found between 18 schemes in domain 3, and the maximum difference for R1 to R3 is 29.13% (found between S1 and S10), 26.68% (found between S1 and S10), and 39.89% (found between S1 and S16), respectively, indicating that for rainfall simulation, the selection of physical parameterizations has a greater influence than the horizontal resolution. This result agrees with the previous studies, and on the contrary, without considering the improvement in the physical parameterizations or initial data, actually, there exists a decrease in the WRF accuracy for rainfall simulation (Li et al. 2016; Avolio et al. 2018; Politi et al. 2018). For example, Duzenli et al. (2020) demonstrated that the results of the rainfall simulation of WRF runs from 9 km domain are closer to observational data than that from 3 km domain. Another study including 96 combinations of physical parameterizations



◀Fig. 5 Spatial distributions of observed and simulated accumulated rainfall (mm) of R1 (S1-S18). Locations of the meteorological stations in the study area are presented as dots, and the color bar represents the 24-h accumulated rainfall amount

carried out by Tian et al. (2017) showed that there is no positive relationship between the performance of WRF runs and horizontal resolution, as WRF rainfall simulations with horizontal grid spacing of 1 km, 3 km, and 9 km show the best performance in 50 cases, 9 cases, and 37 cases, respectively. Improving the horizontal resolution can describe regional features such as terrain and underlying surface conditions that have a significant impact on the accuracy of weather variables prediction. However, the improvement of forecast accuracy by increasing the horizontal resolution is limited (Schwartz et al. 2009; Tian et al. 2017; Li et al. 2014; Duzenli et al. 2020). In WRF, these sub-grid processes are well implemented through physical parameterization schemes, as these physical parameterizations are tailored to certain physical processes with distinctive features (Dasari and Salgado 2015; Efstatouli et al. 2013; Tian et al. 2017; Liu et al. 2020a).

4.2 Influence of CU schemes on rainfall simulation at 3-km resolution

In this section, numerical simulations are conducted with the same model set up as in Section 2.2, with turning off CU schemes at 3-km grid spacing. In order to explore the necessity of using and not using the CU schemes at 3-km grid spacing, the results from 3 km are compared with those obtained from the simulations using CU schemes. In Fig. 3, “R1 + CU” represents the RE value of R1 simulated with CU parameterizations, and “R1” represents the RE value of R1 simulated with turning off CU parameterizations. The performance for simulations with CUs and without CUs varied greatly in different rainfall events. For R1, R2, and R3, there are only 9, 5, and 7 simulations performing better when using CUs than not, respectively. In other words, in most cases, there is not an improvement when using CUs in rainfall simulations at 3-km resolution. However, simulations without CUs can result in a notable improvement for three rainfall events. For example, the RE was significantly reduced by a maximum value of 9.8, 22.29, and 23.36 for three rainfall events. This indicates that the cumulus parameterization scheme may not be needed at 3-km resolution or higher resolutions, as it is enough to explicitly resolve convective processes (Kain et al. 2008; Yu and Lee 2010).

Considering the slight difference between simulations from three domains and the notable improvement when turning off CU schemes in simulating accumulated rainfall, rainfall simulations in domain 3 without using CU schemes for three rainfall events were used as the final results in the follow-up analysis.

4.3 Evaluation of spatial and temporal rainfall simulations

To evaluate the model’s performance in simulating the spatial and temporal patterns of R1, R2, and R3 over the Poyang Lake basin, the Taylor diagram method was used. Figures 4a–c and 8a–c show the spatial and temporal results of R1, R2, and R3, respectively. For spatial rainfall distribution, the metrics are calculated by comparing the 24-h accumulated rainfall simulations with observations at the stations. For temporal rainfall distribution, the metrics are calculated by comparing hourly rainfall simulations with observations at the stations.

In Fig. 4a, all schemes show a positive correlation coefficient with R values ranging from 0.37 to 0.77. Regarding SD, the values of all schemes range from 0.70 to 1.15. The results suggest that most of the schemes show a fair ratio of amplitude against the observation. High differences against the observation were reproduced, as all schemes exhibit C-RMSD in the range of 0.69 to 1.05. Figure 4b shows that all schemes show overall better performance in simulating spatial distributions of R2. The correlation between every WRF simulation and observation is higher than that of R1 and R3, and the R values of all schemes range from 0.67 to 0.88, indicating that the model exhibits the largest similarities to the observation in the spatial distribution. Schemes show similar accuracy in SD, and the SD values range from 0.77 to 1.22. For C-RMSD, the schemes display a lower magnitude of amplitude than the observation, representing relatively better performance against the observation. All the schemes have C-RMSD values in the range of 0.54 to 0.73. Similarly, Fig. 4c shows the performance of all schemes in simulating the rainfall spatial distribution of R3. All schemes show positive R values ranging from 0.24 to 0.64. Most of the schemes have the R values in the range of 0.40 to 0.64, indicating that most of the schemes simulate the spatial rainfall respectively well. In terms of C-RMSD, most of the schemes show large amplitudes against the observation ranging from 0.78 to 1.21. For SD, all schemes have values ranging from 0.48 to 0.95. Most of the schemes have the SD values in the range of 0.60 to 0.95, indicating that most of the schemes simulate the spatial rainfall well. Considering

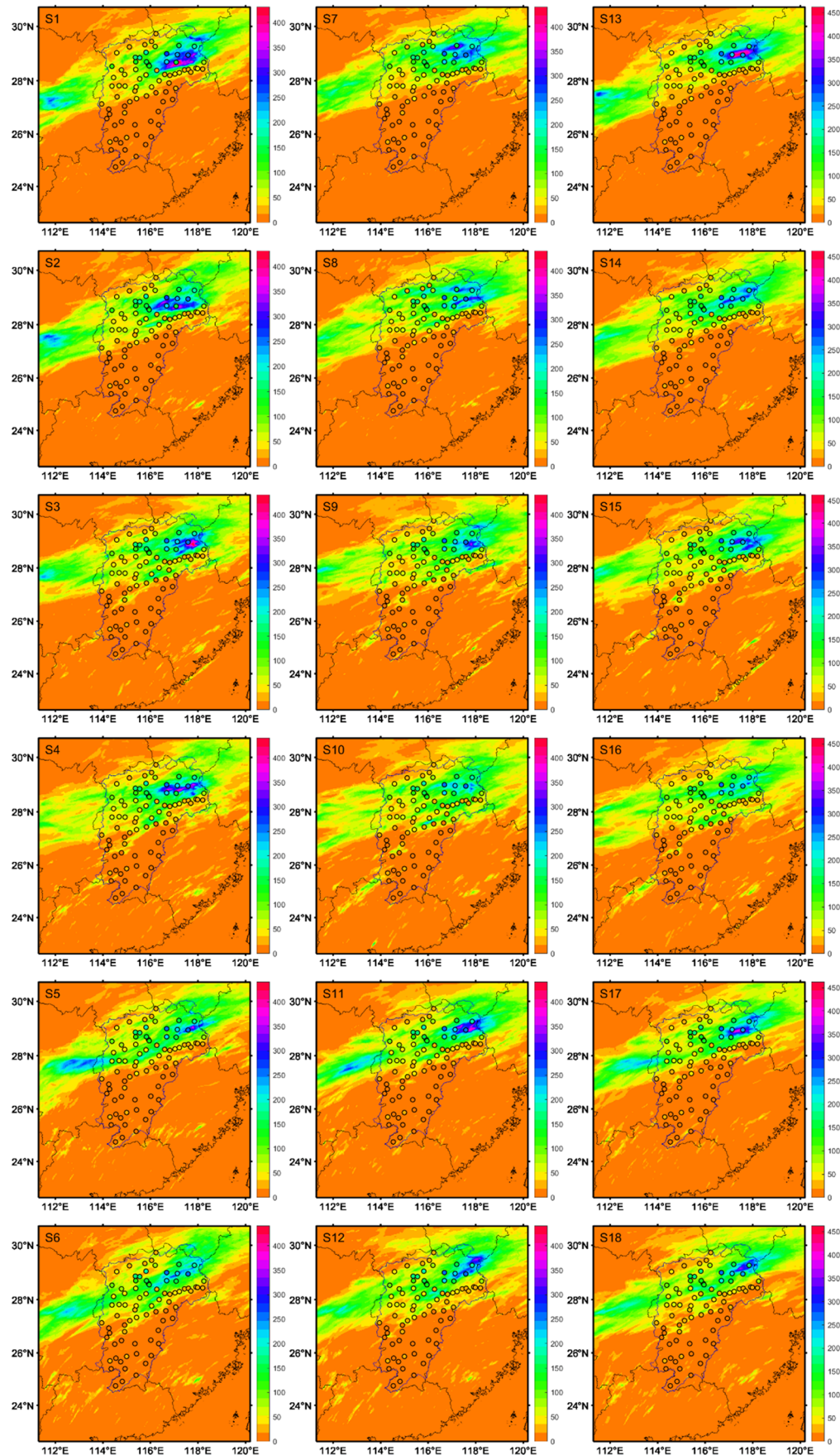


Fig. 6 Spatial distributions of observed and simulated accumulated rainfall (mm) of R2 (S1-S18). Locations of the meteorological stations in the study area are presented as dots, and the color bar represents the 24-h accumulated rainfall amount

three statistics, S8 containing parameterizations of New Thompson and MYJ, S3 containing parameterizations of WSM6 and YSU, and S11 containing parameterizations of New Thompson and YSU show overall the best performance for three rainfall events, respectively.

Figures 5–7 show the spatial patterns of the 24-h accumulated rainfall from 18 WRF simulations and station observation for three rainfall events. For R1 (Fig. 5), although most schemes can simulate the rainfall zone effectively, the maximum rainfall amount is always underestimated. S1 not only succeeded in capturing the heavy zone but also estimated the maximum rainfall amount well. Figure 6 shows that the simulation results of the spatial rainfall patterns for R2 are better than those for R1. The rainfall center is simulated successfully in most schemes, but the maximum rainfall amount tends to be overestimated. Among them, S3 and S13 show better performance than others. While Fig. 7 shows that the rainfall zone was not simulated well and the WRF model failed to reproduce the rainfall magnitude in the Midwest of the study area for R3. This is why R3 has the highest C-RMSD in three rainfall events. For R3, S5, and S11 achieved good results.

Figure 8 shows that all schemes perform worse for three rainfall events in simulating the temporal rainfall distributions than that in simulating the spatial rainfall distributions, as the rainfall is more variable in time than in space (Tian et al. 2017; Tian et al. 2021). In addition, the result shows less change in response to different schemes than that in spatial distribution simulations.

In Fig. 8a, all schemes show low similarities with the observation with R values ranging from 0.04 to 0.19. Regarding SD, the values of all schemes range from 0.85 to 1.32. All the schemes reproduced relatively higher differences against the observation with exhibiting C-RMSD in the range of 1.23 to 1.61. Figure 8b shows that all schemes show overall better performance in simulating temporal distributions of R2. The correlation between most of WRF simulations and observation is higher than that of R1 and R3, and the R values of all schemes range from 0.15 to 0.36, indicating that the model exhibits larger similarities to the observation in the temporal distribution. In addition, most of the schemes reproduced a lower difference against the observation, and the SD values range from 0.92 to 1.09. For C-RMSD, the schemes display a high magnitude of amplitude than the observation, representing relatively better

performance against the observation. All the schemes have C-RMSD values in the range of 1.08 to 1.45. In Fig. 8c, WRF simulations of R3 show the same range in R values from 0.04 to 0.19 as that of R1, indicating that most of the schemes failed to simulate the temporal rainfall. In terms of C-RMSD, most of the schemes show large ratio of deviations and amplitudes against the observation ranging from 1.13 to 1.32. For SD, all schemes have values ranging from 0.71 to 0.93. Considering three statistics, S9 containing parameterizations of New Thompson and YSU, S5 containing parameterizations of WSM6 and YSU, and S6 containing parameterizations of WSM6 and MYJ show overall the best performance for three rainfall events, respectively.

For a detailed comparison, the cumulative curves of the observed and 18 simulated rainfalls for R1, R2, and R3 are shown in Fig. 9a–c, respectively. The shapes of 18 simulated cumulative curves are most consistent with the observed ones for R2, and the simulation results between 18 WRF schemes have a relatively lower difference. Among them, the simulated rainfall occurrences of S11, S9, and S10 always keep step with the observations. While for R1, the simulated processes of 18 schemes are different from the observations. The better results are achieved with S11 and S17 for cumulative rainfall amount simulation, and the rainfall process of S9 is closer with the observation. For R3, the cumulative curves of 18 schemes are all below the observed ones. The schemes of S11, S17, and S12 simulated rainfall processes better than others.

4.4 Sensitivity of the physical parameterizations to spatial and temporal rainfall simulations

In order to explore the sensitivity of MP parameterizations and PBL parameterizations to spatial and temporal rainfall simulations, the Taylor diagram was used. Figure 10 shows the performance of three MPs and two PBLs on spatial and temporal rainfall simulation. For MPs, WSM6 and New Thompson show similar values of three metrics for R1, and Morrison performs worse than others with lower R values and higher C-RMSD values. In simulations of R2 and R3, Morrison and WSM6 show similarity, and they are the best choices for R2 and R3, respectively. There is no consistent conclusion in determining the best MP parameterization for all rainfall events. But the results from PBL parameterizations show that YSU always outperforms than MYJ for three rainfall events, as most simulations with the YSU scheme have relatively higher R values and lower C-RMSD values, and also with SD closer to 1. Results indicate that spatial rainfall simulation is more sensitive to PBL parameterizations, and YSU is the best choice. On the other hand, Fig. 6

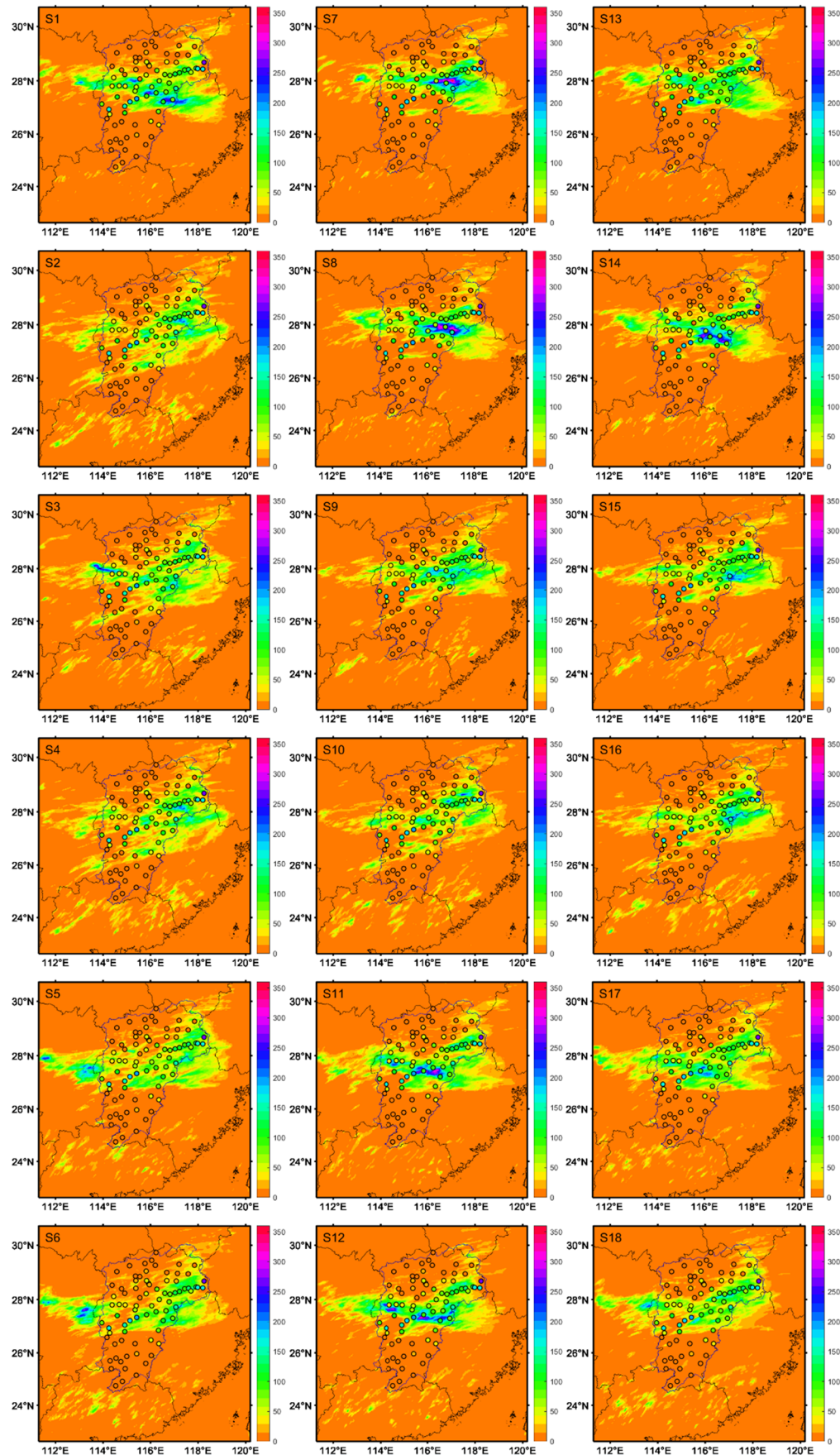


Fig. 7 Spatial distributions of observed and simulated accumulated rainfall (mm) of R3 (S1-S18). Locations of the meteorological stations in the study area are presented as dots, and the color bar represents the 24-h accumulated rainfall amount

shows that the best MP parameterization varies with different rainfall events, while YSU always performs best in temporal simulations for all rainfall events, indicating that physical parameterizations have similar sensitivity to spatial rainfall simulations and temporal rainfall simulations. The planetary boundary layer scheme does not directly affect rainfall simulations but indirectly affects water vapor transport by affecting atmospheric vertical fluxes (Seibert et al. 2000). For different PBLs, the vertical velocity field, moisture flux divergence field, vorticity field, and horizontal wind field divergence all show different characteristics. Previous studies have shown that the planetary boundary layer height (PBLH) is closely related to convective precipitation (Liu and Liang 2010). A higher PBLH leads to stronger vertical mixing in the boundary layer, and vice versa (Adl et al. 2020). Taraphdar et al. (2021) show that regions of stronger instability can lead to decreases in lifting condensation level heights and increases in boundary layer height, suggesting that the boundary layer reaching the cloud base helps to trigger the convection and increase precipitation. In addition, the change of the moisture flux convergence has a good correspondence with the time period and intensity of the rainfall.

In the future research, the influence of YSU and MYJ schemes on physical quantity fields such as the planetary boundary layer heights (m), the lifting condensation level

heights (m), and the lower-level integrated moisture flux convergence in different rainfall processes will be analyzed in detail, so as to further explore the reasons and mechanisms of the differences in simulated precipitation caused by them.

4.5 Overall ranking

It is impossible to determine the best option for each future rainfall event in advance, so a general well parameterization scheme should be given. In order to compare the overall ability of 18 schemes both on spatial and temporal rainfall simulations of three rainfall events, the comprehensive rating index (CRI) was used, and according to which 18 schemes were ranked as shown in Table 3. For each scheme of an individual rainfall event, for example, for S1 of R1, the CRI score is calculated with 18 schemes ($m = 18$) and 6 statistics ($n = 6$), including 3 spatial statistics (R, C-RMSD, SD in spatial Taylor diagram) and 3 temporal statistics (R, C-RMSD, SD in temporal Taylor diagram). For overall rank, for example, for S1, the overall rank is calculated with 18 schemes ($m = 18$) and 3 statistics ($n = 3$), including 3 individual CRI statistics. Results show that the best scheme varies with rainfall events. For example, S1 and S3 rank first in R1 and R2, respectively, while S17 performs the best in R3. Overall, S11, which contains parameterizations of New Thompson and YSU, shows better performance with relatively a higher CRI score, as it ranked in the top 5 for all rainfall events and ranked first in the overall ranks. In addition, S5 containing parameterizations of WSM6 and YSU and S15 containing parameterizations of Morrison and YSU

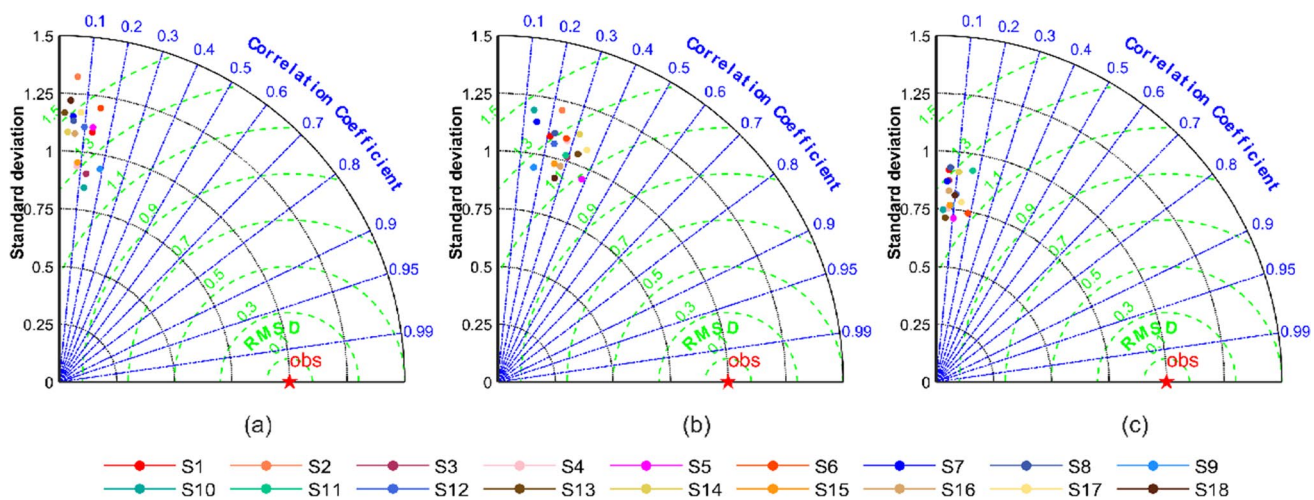
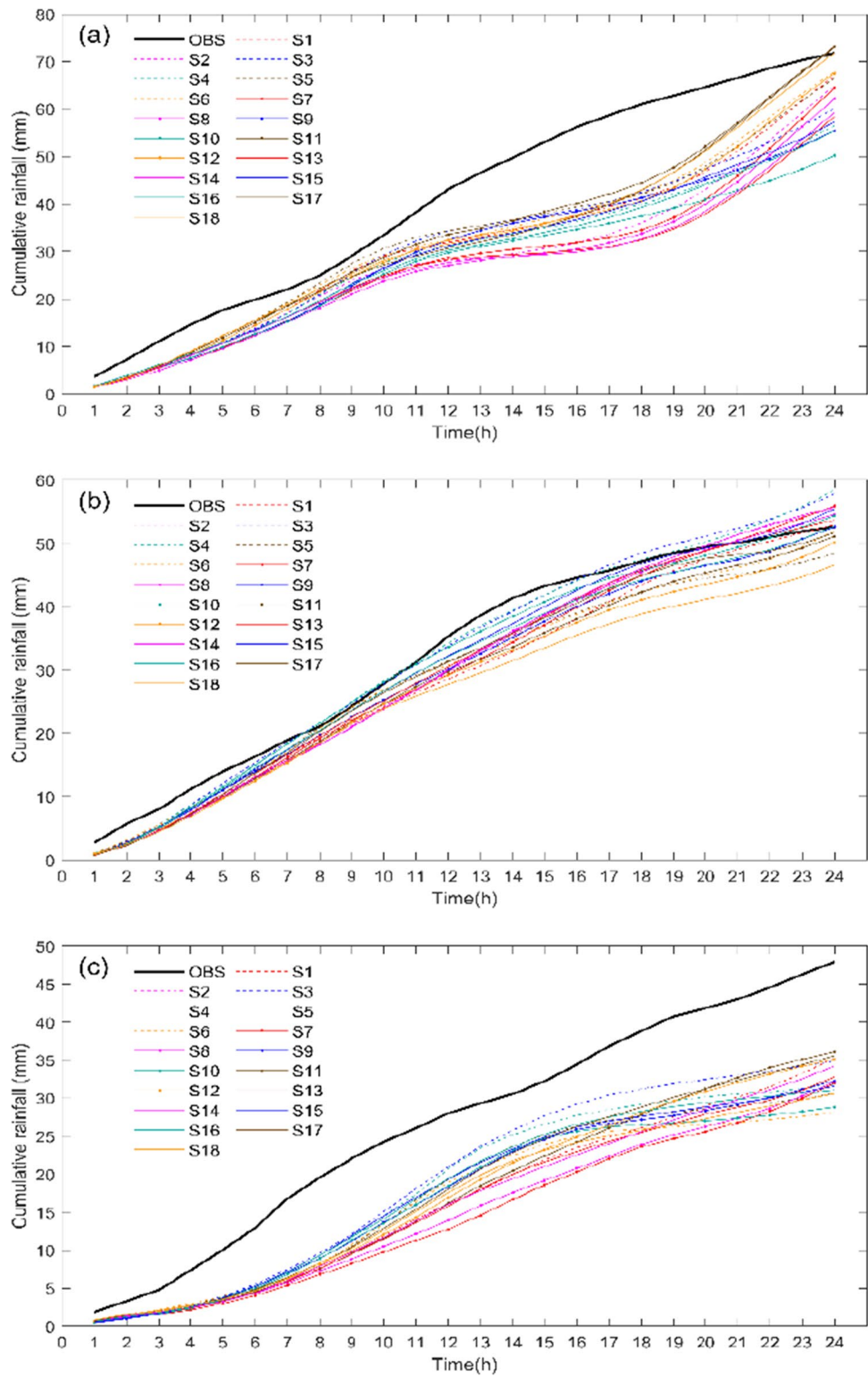


Fig. 8 Taylor diagrams of 18 temporal simulations and observations for R1 (a), R2 (b), and R3 (c)

Fig. 9 Cumulative curves of the observed and 18 simulated areal rainfall of R1 (a), R2 (b), and R3 (c)



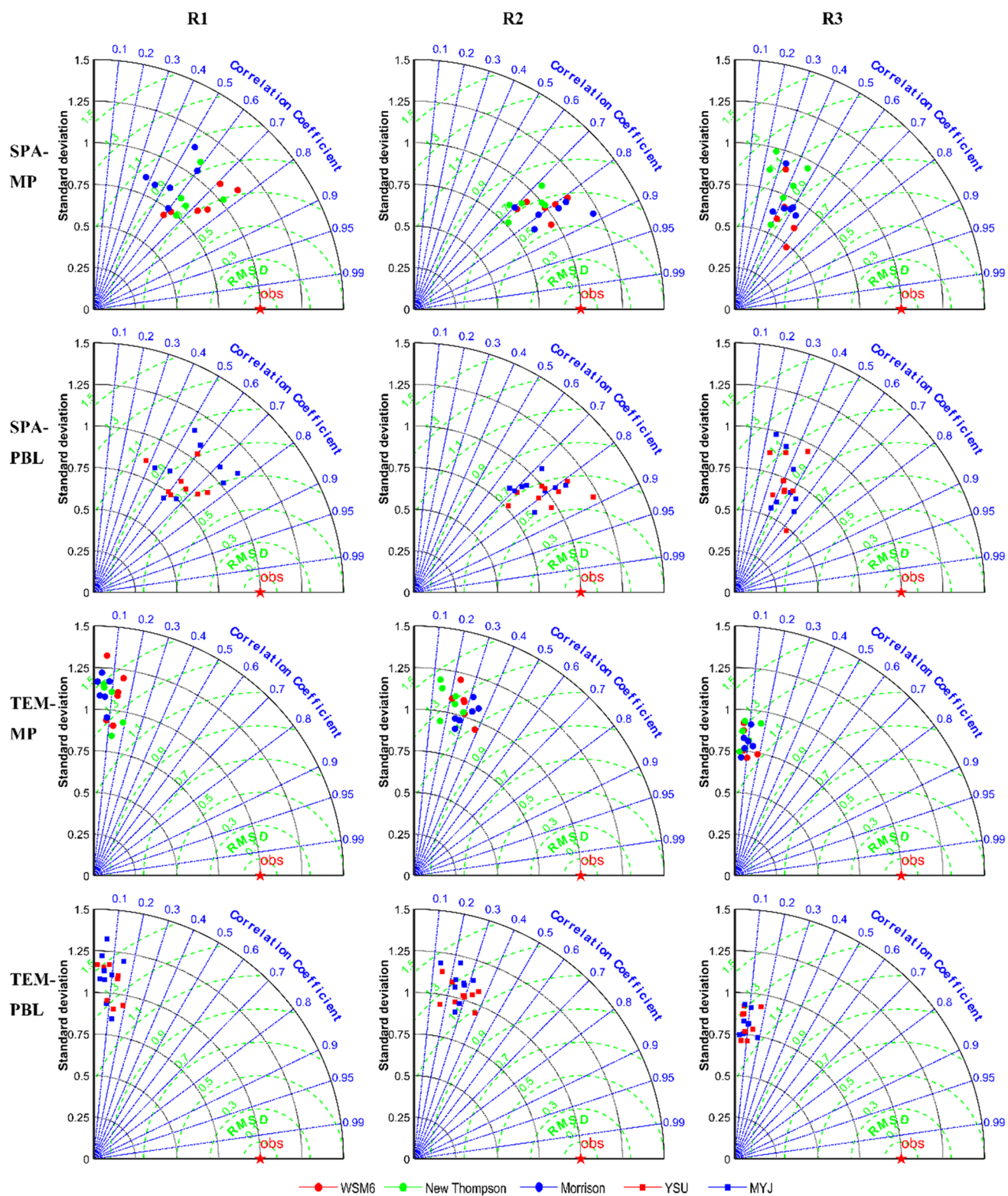


Fig. 10 Taylor diagram for the different physical parameterizations and events in spatiotemporal rainfall simulations. SPA-MP represents the spatial Taylor diagrams for three MP schemes; SPA-PBL represents the spatial Taylor diagrams for two PBL schemes; TEM-

MP represents the temporal Taylor diagrams for three MP schemes; TEM-PBL represents the temporal Taylor diagrams for two PBL schemes

Table 3 Ranks of 18 schemes based on CRI results of rainfall events in both spatial and temporal distribution

Schemes/ranks	R1	R2	R3	Overall rank
S1	1	13	15	10
S2	12	10	11	12
S3	7	1	12	4
S4	10	7	13	11
S5	5	8	4	3
S6	6	12	2	5
S7	15	14	17	18
S8	14	17	14	17
S9	3	15	8	8
S10	8	18	18	16
S11	2	5	3	1
S12	4	16	6	9
S13	17	3	16	15
S14	16	9	10	14
S15	9	6	9	7
S16	11	4	7	6
S17	13	2	1	2
S18	18	11	5	13

also show stable ability in rainfall simulation. They both ranked in the top 9 for all rainfall events. Notably, these well-performing schemes all contain parameterizations of YSU, indicating that the PBL plays an essential role in the accuracy of spatial and temporal rainfall simulations, while the selection of MP parameterizations seems to be less sensitive to the rainfall simulations in the study area. In most cases, no matter which MP scheme is combined with YSU, the PBL scheme always leads to better performance. The important characteristic of MPs is in the vertical structure. The WSM6 scheme utilizes temperature-dependent inception parameters for snow and ice mixing ratios (Hong et al. 2004). Compared with WSM6, the Thompson scheme produces more snow ratio (Jankov et al. 2011). By adding the cloud water change process within a sub-grid scale, the Morrison scheme is able to simulate the vertical water vapor profiles close to the actual observation (Molthan 2011). YSU and MYJ are quite different in terms of how they perform vertical mixing. According to Hong et al. (2006), YSU is more applicable to simulate the convective weather at high resolutions as it uses the “nonlocal K” approach, which is helpful to the vertical transport of physical quantities. This finding is consistent with previous studies. For instance, according to Efstathiou et al. (2013), YSU performs better than MYJ on heavy rainfall prediction in Greece. This further supports

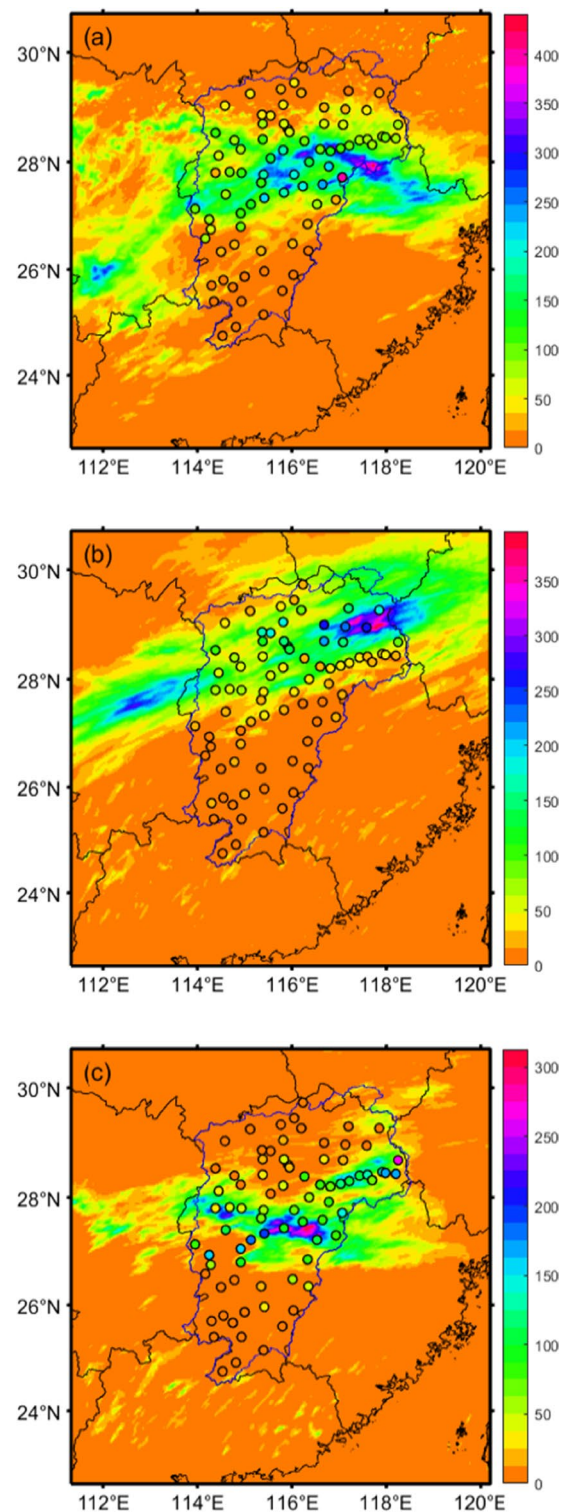


Fig. 11 Spatial distribution of observed and simulated accumulated rainfall (mm) of R1 (a), R2 (b), and R3 (c). Locations of the meteorological stations in the study area are presented as dots, and the color bar represents the 24-h accumulated rainfall amount

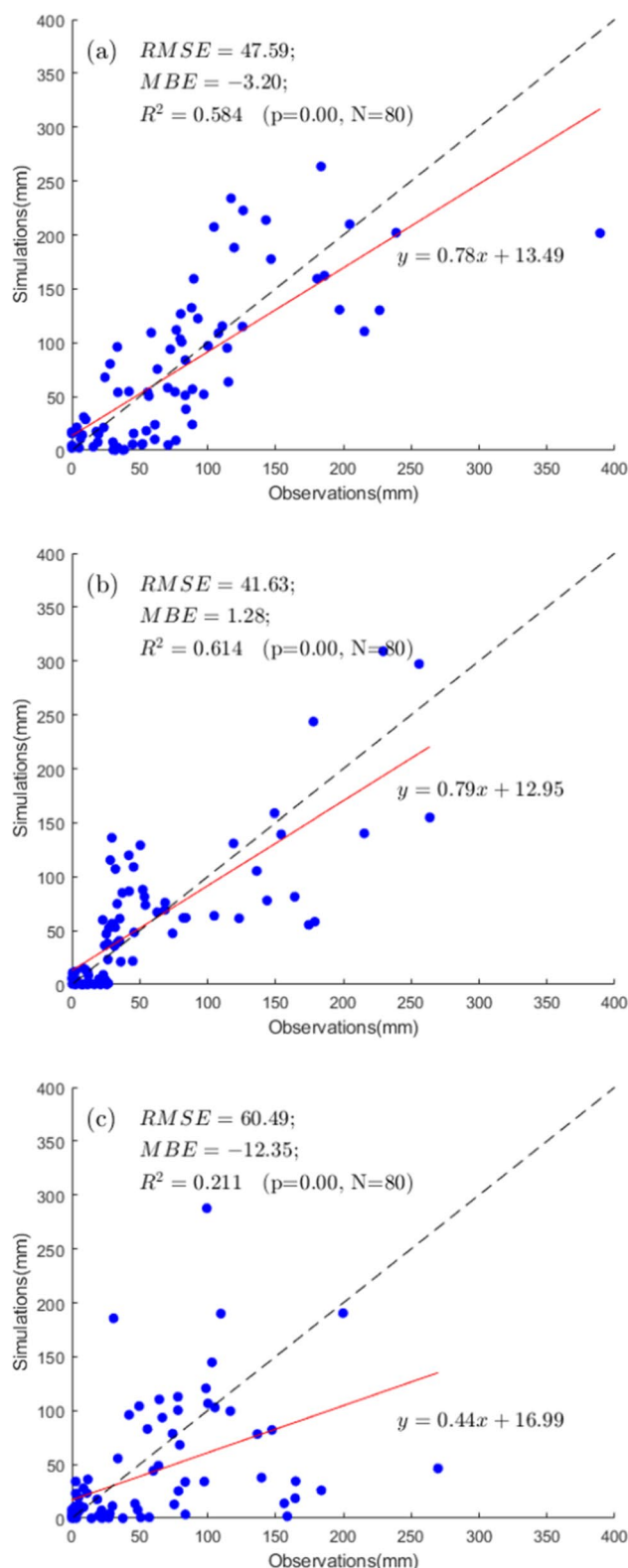


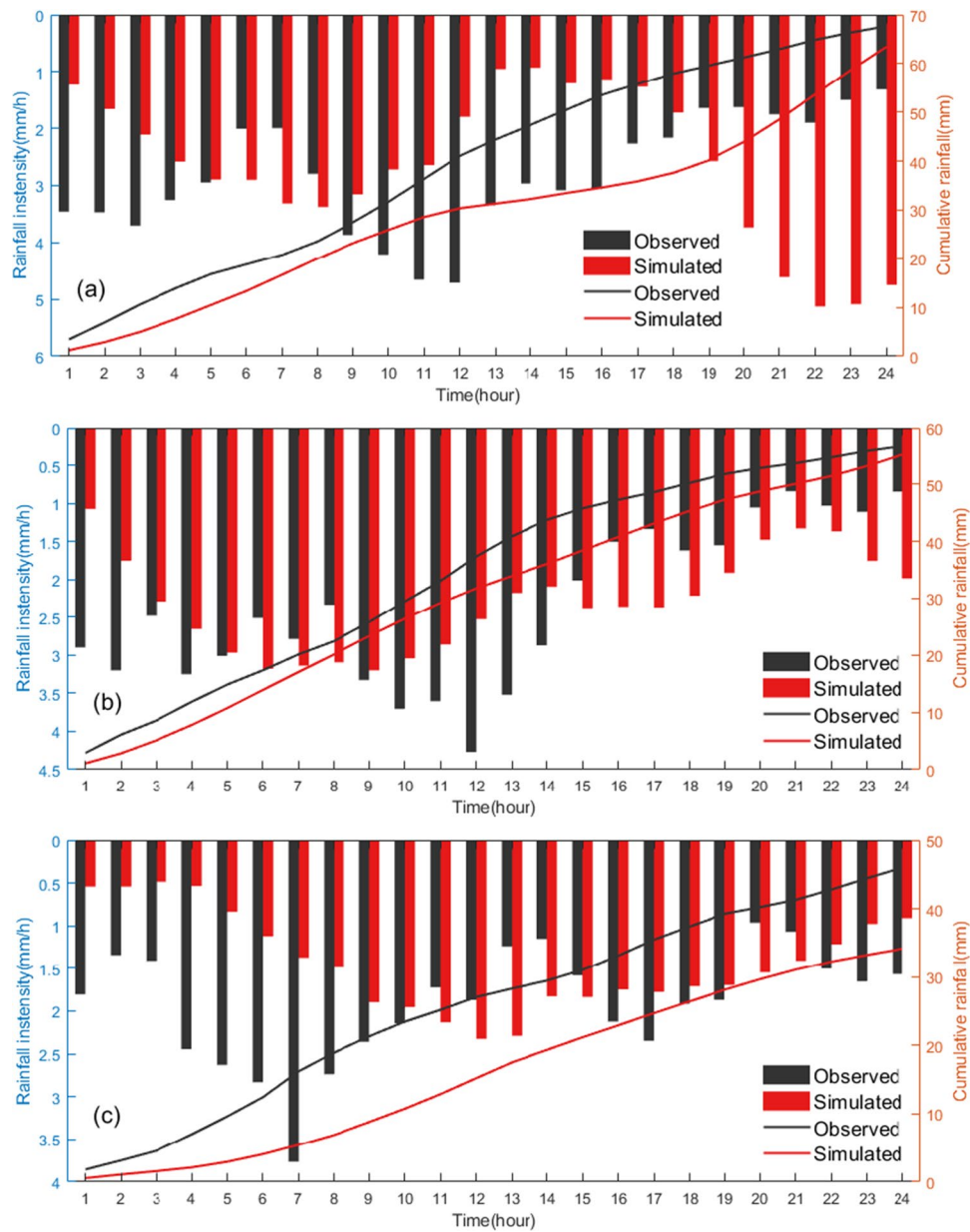
Fig. 12 Scatter plots of observed and simulated accumulated rainfall of R1 (a), R2 (b), and R3 (c)

good agreement with the observations, especially for R2, indicating the reliability of the WRF model in simulating spatial rainfall amounts. The rainfall centers are well simulated for R2, while those of R1 and R3 are not well captured. Rainfall amounts of R1 and R3 are generally underestimated. The maximum difference between observed and simulated is 187.55 mm for R1 and 223.44 mm for R3. The underestimated regions are mainly located in the northern area for the three rainfall simulations. In contrast, those of R2 are generally overestimated, and the maximum difference is 119.17 mm. Overall, results show that the WRF model has a good ability to capture accurate rainfall areas, but there is a limitation in simulating accurate rainfall amounts.

The accuracy of the best spatial simulations for three rainfall events was evaluated using the 80 station observations (Fig. 12). For R1, the RMSE, the MBE (mean bias error), and R^2 of the simulated 24-h rainfall were 47.59, -3.20, and 0.584. For R2, the WRF model simulated the rainfall spatial distribution with the highest accuracy, as the RMSE and the MBE have the minimum values and R^2 has the highest, which were 41.63, 1.28, and 0.614, respectively. For R3, the simulation shows the worst accuracy with a maximum RMSE of 60.49, a higher MBE, and a smaller R^2 (-12.35 and 0.211). The accuracy of the best simulation for different rainfall events also shows differences, indicating the characteristics of the rainfall itself have an influence that cannot be neglected in the WRF model.

Figure 13 shows the cumulative curve and rainfall intensity bars of simulated rainfall from the best scheme (S11) and observed rainfall to display the temporal variation. For the simulation of the rainfall process, the WRF model can simulate the rainfall duration as well as the hourly rainfall was all captured. For R1, most of the time the accumulate rainfall is seriously underestimated, while in the last few hours, the rainfall is highly overestimated (see Fig. 13a). Figure 13b shows that the simulated cumulative curves are most consistent with the observed curve for R2, which indicates that the simulated rainfall occurrences always keep step with the observations. In Fig. 13c, for R3, the rainfall amount is underestimated during the first few hours. Furthermore, the WRF model has a weak ability to capture the occurrence of rainfall peaks for three rainfall events. Among them, only the rainfall peak of R2 was captured a little better than others, while that of R3 was either earlier or later than observed. According to Davis et al. (2022), the temporal lag in WRF-simulated rainfall is due to the inability of

Fig. 13 Rainfall intensity and cumulative curves of the observed and simulated areal rainfall of R1 (a), R2 (b), and R3 (c)



the model to capture the heat exchanges within the study area. In general, the general tendencies show correct, but the actual values are poorly predicted during peak times.

The accuracy of the best temporal simulations was evaluated using the hourly accumulated observed rainfall at a total of 80 stations. From Fig. 14, we can see that, similar to spatial simulations, the simulation results of the WRF model are sorted from the best to the worse, namely R2>R1>R3. For R1, the RMSE, the MBE, and

the necessity to conduct sensitivity study and evaluation of physical parameterizations over specified regions before applying the WRF model for rainfall prediction (Mannan et al. 2013; Pennelly et al. 2014).

Figure 11a–c shows the spatial distribution of the 24-h accumulated rainfall from the WRF simulation simulated by the scheme 11 with the maximum CRI score and station observation for three rainfall events, respectively. The rainfall simulations show a relatively

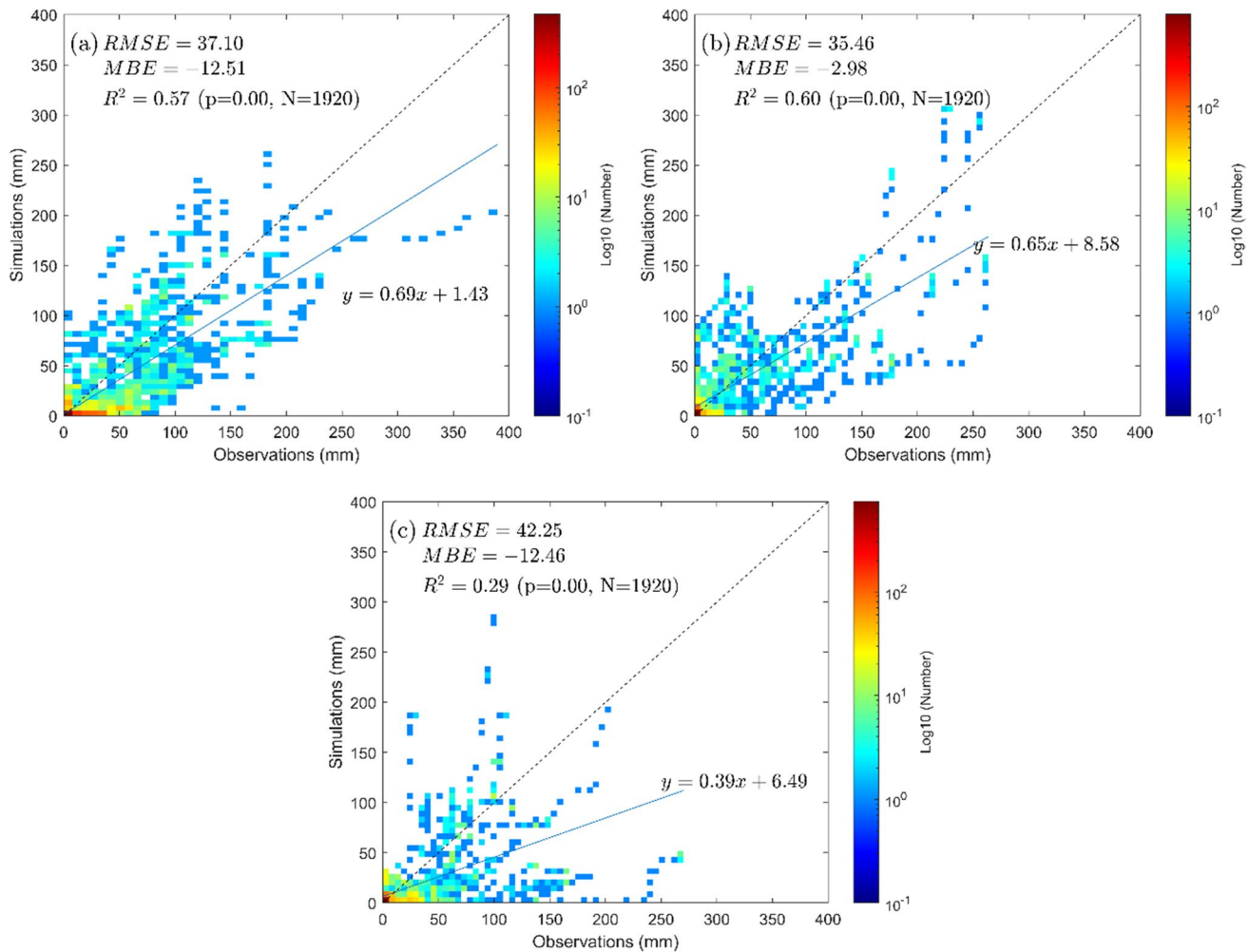


Fig. 14 Scatter plots of the hourly accumulated observed and simulated areal rainfall for R1 (a), R2 (b), and R3 (c)

R^2 of the simulated hourly accumulated rainfall were 37.10, -12.51, and 0.57. For R2, the WRF model simulated the rainfall with the highest accuracy with both the maximum R^2 and the minimum RMSE value, which were 0.60 and 35.46, respectively. For R3, the simulation shows similar accuracy with that for R1 in MBE (-12.46 versus -12.51), but a smaller R^2 (0.29versus 0.57) and a larger RMSE (42.25 versus 37.10).

From the above analysis, the CRI method is proved to be successful in evaluating the performance of the WRF model comprehensively. Although the WRF model tends to underestimate or overestimate rainfall amounts, we believe that the underestimated and overestimated results in time and space are caused not only by the bias errors in the FNL data but also by the inhomogeneity of the complex terrain area. The difficulty of accurately

simulating rainfall with the WRF model has attracted the attention of many researchers. The WRF data assimilation (WRFDA) model is a variational data assimilation system that can provide an improved estimate of the atmospheric state and thus more accurate WRF simulations by ingesting various sources of observations into the WRF products and their respective error statistics. Data assimilation has proven to be a very useful way to largely improve the performance of the WRF model for rainfall simulation when incorporating observations such as weather radar data (Hou et al. 2013; Tian et al. 2017). Besides, it also introduces uncertainties when obtaining station simulations from grid-based results using the interpolation method. Furthermore, we focus on only three MPs and two PBLs, and experiments with other physical parameterizations should be tested.

5 Conclusion

In this study, three rainfall events were simulated using 18 WRF schemes, the performance of which for cumulative rainfall amount and the spatial-temporal distribution over the Poyang Lake basin was evaluated. Furthermore, the influence of individual physical parameterizations on rainfall simulation was also explored. The main conclusions are as follows:

- (1) Physical parameterization is the dominant factor that influences the rainfall simulation, while the horizontal resolution has little impact on the rainfall simulation. Because, when comparing the 3-km resolution simulations against 9 km and 27 km, there is no definite improvement, and differences between them are far less than those between different physical parameterizations. In addition, in most cases, the use of cumulus schemes at 3-km resolution does not result in an improvement in the rainfall forecasts.
- (2) The CRI scores show that the performance of 18 schemes is not always similar in different rainfall events. Overall, scheme 11 containing parameterizations of New Thompson and YSU is the best option for spatial and temporal rainfall simulation. For individual physical parameterization, YSU always outperforms MYJ for three rainfall events in both spatial and temporal rainfall simulations. In addition, schemes 5 and 15 also show better performance. These well-performing schemes all contain YSU, indicating that the selection of PBLs significantly impacts the rainfall simulation and forecasting accuracy in the study area. Using the “nonlocal K” approach, YSU is more suitable for simulating the convective rainfall at high resolutions.
- (3) The PBL parameterizations show an important impact on the accuracy of spatial and temporal rainfall simulation. Among individual parameterizations, YSU is the best choice for PBLs in simulating rainfall over the Poyang Lake basin. Compared with PBLs, the MPs seemed to be of minor importance. According to the overall ranking of three rainfall events computed by CRI, the New Thompson shows better performance for MPs in rainfall event simulations for all rainfall events.

Code availability Not applicable.

Author contributions Jinru Wu wrote the main manuscript text and prepared all the figures and tables. Jianzhong Lu helped perform the analysis with constructive discussions. Xiaoling Chen gave a critical revision of the article. All authors reviewed the manuscript.

Funding This work was funded by the National Key Research and Development Program (2018YFC1506506), the National Natural Science Foundation of China (41971402, 42271354), the Science and Technology Project of Department of Natural Resources of Hubei Province (ZRZY2023KJ41), the Key Research and Development Program of Jiangxi Province (20201BBG71002), and the LIESMARS Special Research Funding.

Data availability FNL data are available at <https://rda.ucar.edu/datasets/ds083.2/#access>. Hourly rainfall data are available at <http://data.cma.cn>.

Declarations

Ethics approval Not applicable.

Consent to participate Not applicable.

Consent for publication Not applicable.

Conflict of interest The authors declare no competing interests.

References

- Adl A, Mn B, Rmga B, Lld A (2020) Sensitivity of meteorological variables on planetary boundary layer parameterization schemes in the WRF-ARW model—ScienceDirect. *Atmos Res* 247:105214. <https://doi.org/10.1016/j.atmosres.2020.105214>
- Afshar MH, Şorman A, Tosunoğlu F et al (2020) Climate change impact assessment on mild and extreme drought events using copulas over Ankara, Turkey. *Theor Appl Climatol* 141. <https://doi.org/10.1007/s00704-020-03257-6>
- Amjad M, Yilmaz MT, Yucel I, Yilmaz KK (2020) Performance evaluation of satellite- and model-based precipitation products over varying climate and complex topography. *J Hydrol* 584:124707. <https://doi.org/10.1016/j.jhydrol.2020.124707>
- Argüeso D, Hidalgo-Muoz JM, Gámiz-Fortis SR, Esteban-Parra MJ, Castro-Díez Y (2011) Evaluation of WRF parameterizations for climate studies over southern Spain using a multistep regionalization. *J Clim* 24(21):5633–5651. <https://doi.org/10.1175/JCLI-D-11-00073.1>
- Avolio E, Federico S (2018) WRF simulations for a heavy rainfall event in southern Italy: verification and sensitivity tests. *Atmos Res* 209:14–35
- Bossioli E, Tombrou M, Dandou A, Athanasopoulou E, Varotsos KV (2009) The role of planetary boundary-layer parameterizations in the air quality of an urban area with complex topography. *Boundary-Layer Meteorol* 131(1):53–72. <https://doi.org/10.1007/s10546-009-9349-7>
- Cassola F, Ferrari F, Mazzino A (2015) Numerical simulations of Mediterranean heavy precipitation events with the WRF model: a verification exercise using different approaches. *Atmos Res* 164:210–225. <https://doi.org/10.1016/j.atmosres.2015.05.010>
- Chawla I, Osuri KK, Mujumdar PP et al (2018) Assessment of the Weather Research and Forecasting (WRF) model for simulation of extreme rainfall events in the upper Ganga Basin. *Hydrol Earth Syst Sci* 22:1095–1117. <https://doi.org/10.5194/hess-2017-533>
- Chen F, Dudhia J (2001) Coupling an advanced land surface–hydrology model with the penn state–NCAR MM5 modeling system. Part I: Model Implementation and Sensitivity. *Monthly Weather Rev*

- 129(4):569–585. [https://doi.org/10.1175/1520-0493\(2001\)129<0569:CAALSH>2.0.CO;2](https://doi.org/10.1175/1520-0493(2001)129<0569:CAALSH>2.0.CO;2)
- Cossu F, Hocke K (2014) Influence of microphysical schemes on atmospheric water in the Weather Research and Forecasting model. *Geosci Model Dev* 7(1). <https://doi.org/10.5194/gmd-7-147-2014>
- Dasari HP, Salgado R (2015) Numerical modelling of heavy rainfall event over Madeira Island in Portugal: sensitivity to different micro physical processes. *Meteorol Appl* 22(1):113–127. <https://doi.org/10.1002/met.1375>
- Davis S, Pentakota L, Sapatarishy N, Mujumdar PP (2022) A flood forecasting framework coupling a high resolution WRF ensemble with an urban hydrologic model. *Front Earth Sci* 10:883842. <https://doi.org/10.3389/feart.2022.883842>
- Di Z, Duan Q, Gong W, Wang C, Gan Y, Quan J, Li J, Miao C, Ye A, Tong C (2015) Assessing WRF model parameter sensitivity: a case study with 5 day summer precipitation forecasting in the Greater Beijing Area. *Geophys Res Lett* 42:579–587. <https://doi.org/10.1002/2014GL061623>
- Dudhia J (1989) Numerical study of convection observed during the winter monsoon experiment using a mesoscale two-dimensional model. *J Atmos* 46(20):3077–3107. [https://doi.org/10.1175/1520-0469\(1989\)046<3077:NSOCOD>2.0.CO;2](https://doi.org/10.1175/1520-0469(1989)046<3077:NSOCOD>2.0.CO;2)
- Dozenli E, Yucel I, Pilatin H, Yilmaz MT (2020) Evaluating the performance of a WRF initial and physics ensemble over Eastern Black Sea and Mediterranean regions in Turkey. *Atmos Res* 248:105184. <https://doi.org/10.1016/j.atmosres.2020.105184>
- Dyer J, Zarzar C, Amburn P, Dumais R, Raby J, Smith JA (2016) Defining the influence of horizontal grid spacing on ensemble uncertainty within a regional modeling framework. *Weather Forecast* 31(6):1997–2017. <https://doi.org/10.1175/WAF-D-16-0030.1>
- Efstathiou GA, Zoumakis NM, Melas D, Lolis CJ, Kassomenos P (2013) Sensitivity of WRF to boundary layer parameterizations in simulating a heavy rainfall event using different microphysical schemes. Effect on large-scale processes. *Atmos Res* 132:125–143. <https://doi.org/10.1016/j.atmosres.2013.05.004>
- Flaounas E, Bastin S, Janicot S (2011) Regional climate modelling of the 2006 West African monsoon: sensitivity to convection and planetary boundary layer parameterisation using WRF. *Clim Dyn* 36(5):1083–1105. <https://doi.org/10.1007/s00382-010-0785-3>
- Grell GA, Devenyi D (2002) A generalized approach to parameterizing convection combining ensemble and data assimilation techniques. *Geophys Res Lett* 29. <https://doi.org/10.1029/2002GL015311>
- Hasan MA, Saiful Islam AKM (2018) Evaluation of microphysics and cumulus schemes of WRF for forecasting of heavy monsoon rainfall over the southeastern hilly region of Bangladesh. *Pure Appl Geophys* 175:4537–4566. <https://doi.org/10.1007/s0024-018-1876-z>
- Hong SY, Dudhia J, Chen SH (2004) A revised approach to ice microphysical processes for the bulk parameterization of clouds and precipitation. *Mon Weather Rev* 132(1):103–120
- Hong SY, Lee JW (2009) Assessment of the WRF model in reproducing a flash-flood heavy rainfall event over Korea. *Atmos Res* 93(4):818–831. <https://doi.org/10.1016/j.atmosres.2009.03.015>
- Hong SY, Lim JOJ (2006) The WRF single-moment 6-class microphysics scheme (WSM6). *J Korean Meteor Soc* 42:129–151
- Hong SY, Noh Y, Dudhia J (2006) A new vertical diffusion package with an explicit treatment of entrainment processes. *Month Weather Rev* 134(9):2318–2341. <https://doi.org/10.1175/MWR3199.1>
- Hou T, Kong F, Chen X, Lei H (2013) Impact of 3DVAR Data assimilation on the prediction of heavy rainfall over Southern China. *Adv Meteorol*:1–17. <https://doi.org/10.1155/2013/129642>
- Houze RA, Chen SS, Lee WC, Rogers FR, Moore JA, Stossmeister GJ, Bell MM, Cetrone J, Zhao W, Brodzik SR (2006) The hurricane rainband and intensity change experiment: observations and modeling of hurricanes Katrina, Ophelia, and Rita. *Bull Am Meteorol Soc* 87(11):1503–1522. <https://doi.org/10.1175/BAMS-87-11-1503>
- Huang D, Gao S (2017) Impact of different cumulus convective parameterization schemes on the simulation of precipitation over China. *Tellus A: Dyn Meteorol Oceanograph* 69(1):1406264. <https://doi.org/10.1080/16000870.2017.1406264>
- Janjic ZI (1994) The Step–Mountain Eta Coordinate Model: further developments of the convection, viscous sublayer, and turbulence closure schemes. *Mon Weather Rev* 122:927–945. [https://doi.org/10.1175/1520-0493\(1994\)122<0927:TSMECM>2.0.CO;2](https://doi.org/10.1175/1520-0493(1994)122<0927:TSMECM>2.0.CO;2)
- Janjic ZI (2001) Nonsingular implementation of the Mellor–Yamada Level 2.5 scheme in the NCEP Meso Model. ncep office note,437:61
- Jankov I, Grasso LD, Sengupta M, Neiman PJ, Zupanski D, Zupanski M, Lindsey D, Hillger DW, Birkenheuer DL, Brummer R, Yuan H (2011) An evaluation of five ARW-WRF microphysics schemes using synthetic GOES imagery for an atmospheric river event affecting the California coast. *J Hydrometeorol* 12(4):618–633
- Jarvis D, Stoeckl N, Chaiechi T (2013) Applying econometric techniques to hydrological problems in a large basin: quantifying the rainfall–discharge relationship in the Burdekin, Queensland, Australia. *J Hydrol* 496:107–121. <https://doi.org/10.1016/j.jhydrol.2013.04.043>
- Jiang Z, Li W, Xu J, Li L (2015) Extreme precipitation indices over China in CMIP5 models. Part I: Model evaluation. *J Clim* 28(21):8603–8619. <https://doi.org/10.1175/JCLI-D-15-0099.1>
- Kain JS (2004) The Kain–Fritsch convective parameterization: an update. *J Appl Meteorol* 43(1):170–81
- Kain JS, and J. M. Fritsch (1993) Convective parameterization in mesoscale models: the Kain–Fritsch scheme. *The Representation of Cumulus Convection in Numerical Models*, Meteor. Monogr., Vol. 46, Amer. Meteor. Soc., 165–170
- Kain JS, Weiss SJ, Bright DR, Baldwin ME, Levit JJ, Carbin GW, Schwartz CS, Weisman ML, Droegemeier KK, Weber DB, Thomas KW (2008) Some practical considerations regarding horizontal resolution in the first generation of operational convection-allowing NWP. *Weather Forecast* 23(5):931–952. <https://doi.org/10.1175/WAF2007106.1>
- Kain JS, Xue M, Coniglio MC, Weiss SJ, Kong F, Jensen TL, Brown BG, Gao J, Brewster K, Thomas KW (2010) Assessing advances in the assimilation of radar data and other mesoscale observations within a collaborative forecasting-research environment. *Weather Forecast* 25(5):1510–1521. <https://doi.org/10.1175/2010WAF2222405.1>
- Kan Y, Liu C, Liu Y, Zhou C (2015) Evaluation of WRF microphysics and cumulus parameterization schemes in simulating a heavy rainfall event over Yangtze River delta (SPIE). <https://doi.org/10.1117/12.2185766>
- Kim JH, Shin DB, Kummerow C (2013) Impacts of a priori databases using six WRF microphysicsschemes on passive microwave rainfall retrievals. *J Atmos Ocean Technol* 30(10):2367–2381. <https://doi.org/10.1175/JTECH-D-12-00261.1>
- Li LF, Li WH, Jin JM (2014) Improvements in WRF simulation skills of southeastern United States summer rainfall: physical parameterization and horizontal resolution. *Clim Dyn* 43(7–8):2077–2091. <https://doi.org/10.1007/s00382-013-2031-2>
- Li X, Pu Z (2008) Sensitivity of numerical simulation of early rapid intensification of Hurricane Emily (2005) to cloud microphysical and planetary boundary layer parameterizations. *Mon Weather Rev* 136(12):4819–4838. <https://doi.org/10.1175/2008MWR2366.1>
- Li X, Pu Z (2009) Sensitivity of numerical simulations of the early rapid intensification of hurricane Emily to cumulus parameterization schemes in different model horizontal resolutions. *J Meteorol*

- SocJapan Ser II 87(3):403–421. <https://doi.org/10.2151/jmsj.87.403>
- Li Y, Lu G, Wu Z, He H, Shi J, Ma Y, Weng S (2016) Evaluation of optimized WRF precipitation forecast over a complex topography region during flood season. *Atmosphere* 7(11):145. <https://doi.org/10.3390/atmos7110145>
- Liang D, Lu J, Chen X, Liu C, Lin J (2020) An investigation of the hydrological influence on the distribution and transition of wetland cover in a complex lake–floodplain system using time-series remote sensing and hydrodynamic simulation. *J Hydrol* 587:125038. <https://doi.org/10.1016/j.jhydrol.2020.125038>
- Lim KSS, Hong SY (2010) Development of an effective double-moment cloud microphysics scheme with prognostic cloud condensation nuclei (CCN) for weather and climate Models. *Mon Weather Rev* 138(5):1587–1612. <https://doi.org/10.1175/2009MWR2968.1>
- Lin YL, Farley RD, Orville HD (1983) Bulk parameterization of the snow field in a cloud model. *J Appl Meteorol* 22(6):1065–1092. [https://doi.org/10.1175/1520-0450\(1983\)022<1065:BPOTSF>2.0.CO;2](https://doi.org/10.1175/1520-0450(1983)022<1065:BPOTSF>2.0.CO;2)
- Ling T, Xiao W, Deng D (2020) Analysis of the cause of a continuous rainstorm in Jiangxi in early June 2019. *Meteorology and Disaster Reduction Research* 43(4):284–291
- Litta AJ, Mohanty UC, Das S, Idicula SM (2012) Numerical simulation of severe local storms over east India using WRF-NMM mesoscale model. *Atmos Res* 116:161–184. <https://doi.org/10.1016/j.atmosres.2012.04.015>
- Liu S, Liang XZ (2010) Observed diurnal cycle climatology of planetary boundary layer height. *J Clim* 23(21):5790–5809. <https://doi.org/10.1175/2010JCLI3552.1>
- Liu Y, Chen X, Li Q, Yang J, Li L, Wang T (2020a) Impact of different microphysics and cumulus parameterizations in WRF for heavy rainfall simulations in the central segment of the Tianshan Mountains, China. *Atmos Res* 244:105052. <https://doi.org/10.1016/j.atmosres.2020.105052>
- Liu Z, Lu J, Huang J, Chen X, Zhang L (2020b) Projection of reference crop evapotranspiration under future climate change in Poyang Lake watershed, China. *J Hydrol Eng* 26(1):05020042. [https://doi.org/10.1061/\(ASCE\)HE.1943-5584.0002020](https://doi.org/10.1061/(ASCE)HE.1943-5584.0002020)
- Madala S, Satyanarayana ANV, Rao TN (2014) Performance evaluation of PBL and cumulus parameterization schemes of WRF ARW model in simulating severe thunderstorm events over Gadanki MST radar facility—case study. *Atmos Res* 139:1–17. <https://doi.org/10.1016/j.atmosres.2013.12.017>
- Mannan MA, Chowdhury MAM, Karmakar S (2013) Application of NWP model in prediction of heavy rainfall in Bangladesh. *Proc Eng* 56:667–675. <https://doi.org/10.1016/j.proeng.2013.03.176>
- Maussion F, Scherer D, Finkelnburg R, Richters J, Yang W, Yao T (2011) WRF simulation of a precipitation event over the Tibetan Plateau, China – an assessment using remote sensing and ground observations. *Hydrol Earth Syst Sci* 15(6):1795–1817. <https://doi.org/10.5194/hess-15-1795-2011>
- Misenis C, Zhang Y (2010) An examination of sensitivity of WRF/Chem predictions to physical parameterizations, horizontal grid spacing, and nesting options. *Atmos Res* 97(3):315–334. <https://doi.org/10.1016/j.atmosres.2010.04.005>
- Mlawer EJ, Taubman SJ, Brown PD et al (1997) Radiative transfer for inhomogeneous atmosphere: RRTM. *J Geophys Res Atmos* 102(14):16663–16682. <https://doi.org/10.1029/97JD00237>
- Mohanty MP, Sherly MA, Ghosh S, Karmakar S (2020) Tide-rainfall flood quotient: an incisive measure of comprehending a region's response to storm-tide and pluvial flooding. *Environ Res Lett* 15(6). <https://doi.org/10.1088/1748-9326/ab8092>
- Molthan AL (2011) Evaluating the performance of single and double moment microphysics schemes during a synoptic-scale snowfall event. AMS conferences on weather and forecasting/numerical weather prediction, Seattle, WA
- Morrison H, Thompson G, Tatarki V (2009) Impact of cloud micro-physics on the development of trailing stratiform precipitation in a simulated squall line: comparison of one- and two-moment schemes. *Mon Wea Rev* 137:991–1007. <https://doi.org/10.1175/2008MWR2556.1>
- Muis S, Verlaan M, Winsemius HC, Aerts JC, Ward PJ (2016) A global reanalysis of storm surges and extreme sea levels. *Nat Commun* 7(1):11969. <https://doi.org/10.1038/ncomms11969>
- Nicótina L, Alessi CE, Rinaldo A, Marani M (2008) On the impact of rainfall patterns on the hydrologic response. *Water Resour Res* 44(12). <https://doi.org/10.1029/2007WR006654>
- Patel P, Ghosh S, Kaginalkar A, Islam S, Karmakar S (2019) Performance evaluation of WRF for extreme flood forecasts in a coastal urban environment. *Atmos Res* 223(7):39–48. <https://doi.org/10.1016/j.atmosres.2019.03.005>
- Pei LS, Moore N, Zhong SY et al (2014) WRF model sensitivity to land surface model and cumulus parameterization under short-term climate extremes over the southern great plains of the United States. *J Clim* 27:7703–7724. <https://doi.org/10.1175/JCLI-D-14-00015.1>
- Pennelly C, Reuter G, Flesch T (2014) Verification of the WRF model for simulating heavy precipitation in Alberta. *Atmos Res* 135:172–192. <https://doi.org/10.1016/j.atmosres.2013.09.004>
- Piciullo L, Calvello M, Cepeda J (2018) Territorial early warning systems for rainfall-induced landslides. *Earth-Sci Rev* 179:228–247. <https://doi.org/10.1016/j.earscirev.2018.02.013>
- Pieri AB, von Hardenberg J, Parodi A, Provenzale A (2015) Sensitivity of precipitation statistics to resolution, microphysics, and convective parameterization: a case study with the high-resolution WRF climate model over Europe. *J Hydrometeorol* 16(4):1857–1872. <https://doi.org/10.1175/JHM-D-14-0221.1>
- Politi N, Nastos PT, Sfetsos A, Vlachogiannis D, Dalezios NR (2018) Evaluation of the AWR-WRF model configuration at high resolution over the domain of Greece. *Atmos Res* 208:229–245. <https://doi.org/10.1016/j.atmosres.2017.10.019>
- Prein AF, Holland GJ, Rasmussen RM, Done J, Ikeda K, Clark MP, Liu CH (2013) Importance of regional climate model grid spacing for the simulation of heavy precipitation in the Colorado headwaters. *J Clim* 26(13):4848–4857. <https://doi.org/10.1175/jcli-d-12-00727.1>
- Que LJ, Que WL, Feng JM (2016) Intercomparison of different physics schemes in the WRF model over the Asian summer monsoon region. *Atmos Ocean Sci Lett* 9(3):169–177. <https://doi.org/10.1080/16742834.2016.1158618>
- Rasmussen R, Liu C, Ikeda K, Gochis D, Yates D, Chen F, Gutmann E (2011) High-resolution coupled climate runoff simulations of seasonal snowfall over Colorado: a process study of current and warmer climate. *J Clim* 24(12):3015–3048. <https://doi.org/10.1175/2010jcli3985.1>
- Sanchez N, Martinez-Fernandez J, Scaini A, Perez-Gutierrez C (2012) Validation of the SMOS L2 soil moisture data in the REMEDHUS network (Spain). *IEEE Trans Geosci Remote Sens* 50(5):1602–1611. <https://doi.org/10.1109/tgrs.2012.2186971>
- Sathyamadhan A, Prabha TV, Balaji B, Resmi EA, Karipot A (2017) Evaluation of WRF PBL parameterization schemes against direct observations during a dry event over the Ganges valley. *Atmos Res* 193:125–141. <https://doi.org/10.1016/j.atmosres.2017.02.016>
- Schiermeier Q (2011) Increased flood risk linked to global warming. *Nature* 470:316–316. <https://doi.org/10.1038/470316a>
- Schwartz CS, Kain JS, Weiss SJ, Xue M, Bright DR, Kong F, Thomas KW, Levitt JJ, Coniglio MC (2009) Next-day convection-allowing WRF model guidance: a second look at 2-km versus 4-km grid spacing. *Mon Weather Rev* 137(10):3351–3372. <https://doi.org/10.1175/2009MWR2924.1>

- Seibert P, Beyrich F, Gryning SE, Joffre S, Rasmussen A, Tercier P (2000) Review and intercomparison of operational methods for the determination of the mixing height. *Atmos Environ* 34(7):1001–1027. [https://doi.org/10.1016/S1352-2310\(99\)00349-0](https://doi.org/10.1016/S1352-2310(99)00349-0)
- Shrestha DL, Robertson DE, Wang QJ, Pagano TC, Hapuarachchi HAP (2013) Evaluation of numerical weather prediction model precipitation forecasts for shortterm streamflow forecasting purpose. *Hydrol Earth Syst Sci*. <https://doi.org/10.5194/hess-17-1913-2013>
- Sikder S, Hossain F (2016) Assessment of the Weather Research and Forecasting model generalized parameterization schemes for advancement of precipitation forecasting in monsoon-driven river basins. *J Adv Model Earth Syst* 8(3):1210–1228. <https://doi.org/10.1002/2016MS000678>
- Singh KS, Bonthu S, Purvaja R et al (2018) Prediction of heavy rainfall over Chennai Metropolitan City, Tamil Nadu, India: impact of microphysical parameterization schemes. *Atmos Res* 202:219–234. <https://doi.org/10.1016/j.atmosres.2017.11.028>
- Skamarock WC, Klemp JB, Dudhia J, Gill DO, Barker DM, Wang W et al (2008) A Description of the Advanced Research WRF Version 3. Available from NCAR; P.O. BOX 3000. Boulder CO 88:7–25
- Song HJ, Shin S, Ha JH, Lim S (2017) The advantages of hybrid 4DEnVar in the context of the forecast sensitivity to initial conditions. *J Geophys Res Atmos*. <https://doi.org/10.1002/2017JD027598>
- Spinoni J, Barbosa P, Bucchignani E et al (2020) Future global meteorological drought hot spots: a study based on CORDEX Data. *J Clim* 33:3635–3661. <https://doi.org/10.1175/JCLI-D-19-0084.1>
- Sun SQ, Zhen J, Xu AH, Chen YH (2015) A study on the causes of heavy rainfall process in northern Jiangxi. *Meteorol Disaster Reduct Res* 38(01):25–36
- Sunny Lim KS, Hong SY, Yoon JH et al (2014) Simulation of the summer monsoon rainfall over east Asia using the NCEP GFS cumulus parameterization at different horizontal resolutions. *Weather Forecast* 29(5):140507123951001. <https://doi.org/10.1175/WAF-D-13-00143.1>
- Tang LL, Cai XB, Gong WS, Lu JZ, Yu GL (2018) Increased vegetation greenness aggravates water conflicts during lasting and intensifying drought in the Poyang Lake watershed, China. *Forests*, 9(1):24. <https://doi.org/10.3390/f9010024>
- Taraphdar S, Pauluis OM (2021) Impact of planetary boundary layer and cloud microphysics on the sensitivity of monsoon precipitation using a gray one regional model. *Earth Space Sci* 8(5):e2020EA001535
- Taraphdar S, Pauluis OM, Xue L, Liu C, Rasmussen R, Ajayamohan RS (2021) WRF gray zone simulations of precipitation over the Middle-East and the UAE: impacts of physical parameterizations and resolution. *J Geophys Res: Atmos* 126:e2021JD034648. <https://doi.org/10.1029/2021JD034648>
- Taylor KE (2001) Summarizing multiple aspects of model performance in a single diagram. *J Geophys Res: Atmos* 106(D7):7183–7192. <https://doi.org/10.1029/2000jd900719>
- Thompson G, Rasmussen RM, Manning K (2004) Explicit forecasts of winter precipitation using an improved bulk microphysics scheme. Part I: Description and sensitivity analysis. *Mon Weather Rev* 132:519–542. <https://doi.org/10.1175/2008MWR2387.1>
- Tian J, Liu J, Wang J, Li C, Yu F, Chu Z (2017) A spatio-temporal evaluation of the WRF physical parameterizations for numerical rainfall simulation in semi-humid and semi-arid catchments of Northern China. *Atmos Res* 191:141–155. <https://doi.org/10.1016/j.atmosres.2017.03.012>
- Tian J, Liu R, Ding L, Guo L, Liu Q (2021) Evaluation of the WRF physical parameterisations for Typhoon rainstorm simulation in southeast coast of China. *Atmos Res* 247:105130. <https://doi.org/10.1016/j.atmosres.2020.105130>
- Verma S, Panda J, Rath SS (2021) Role of PBL and microphysical parameterizations during WRF simulated monsoonal heavy rainfall episodes over Mumbai. *Pure Appl Geophys* 178:3673–3702. <https://doi.org/10.1007/s0024-021-02813-z>
- Yang QY, Yu ZB, Wei JH et al (2020) Performance of the WRF model in simulating intense precipitation events over the Hanjiang River Basin, China—a multi-physics ensemble approach. *Atmos Res* 248. <https://doi.org/10.1016/j.atmosres.2020.105206>
- Yu X, Lee TY (2010) Role of convective parameterization in simulations of a convection band at grey-zone resolutions. *Tellus A: Dyn Meteorol Oceanograph* 62(5):617–632. <https://doi.org/10.1111/j.1600-0870.2010.00470.x>
- Zhai P, Zhang X, Wan H, Pan X (2005) Trends in total precipitation and frequency of daily precipitation extremes over China. *J Clim* 18(7):1096–1108. <https://doi.org/10.1175/JCLI-3318.1>
- Zhou ZG, Jiang YQ, Zhang GY, Zhang WJ, Wang CL (2012) Numerical simulation on a heavy rainfall event over Jiangxi province. *Meteorol Environ Res* 3(12):8–12
- Zhuo L, Dai Q, Han D, Chen N, Zhao B (2019) Assessment of simulated soil moisture from WRF Noah, Noah-MP, and CLM land surface schemes for landslide hazard application. *Hydrol Earth Syst Sci* 23(10):4199–4218. <https://doi.org/10.5194/hess-23-4199-2019>

Publisher's note Springer Nature remains neutral with regard to jurisdictional claims in published maps and institutional affiliations.

Springer Nature or its licensor (e.g. a society or other partner) holds exclusive rights to this article under a publishing agreement with the author(s) or other rightsholder(s); author self-archiving of the accepted manuscript version of this article is solely governed by the terms of such publishing agreement and applicable law.